ESCUELA POLITÉCNICA NACIONAL

FACULTAD DE INGENIERÍA MECÁNICA

PARAMETRIC MODEL FOR WEIGHT AND PERFORMANCE ASSESSMENT OF AN ELECTRIC-POWERED UNMANNED AERIAL VEHICLE FOR THE ANDEAN REGION

TRABAJO DE TITULACIÓN PREVIO A LA OBTENCIÓN DEL TÍTULO DE INGENIERO MECÁNICO

ORLANDO DAVID CALLE LANDÁZURI
orlando.calle@epn.edu.ec

DIRECTOR: Esteban Alejandro Valencia Torres, Ph.D.
esteban.valencia@epn.edu.ec

CODIRECTOR: Víctor Hugo Hidalgo Díaz, D.Sc.
victor.hidalgo@epn.edu.ec

Quito, noviembre 2017

DECLARACIÓN

Yo Orlando David Calle Landázuri, declaro que el trabajo aquí descrito es de mi autoría; que no ha sido previamente presentado para ningún grado o calificación profesional; y, que he consultado las referencias bibliográficas que se incluyen en este documento.

La Escuela Politécnica Nacional, puede hacer uso de los derechos correspondientes a este trabajo, según lo establecido por la Ley de Propiedad Intelectual, por su Reglamento y por la normatividad institucional vigente.

_____

Orlando David Calle Landázuri

CERTIFICACIÓN

Certifico que el presente trabajo fue desarrollado por el Sr. Orlando David Calle Landázuri bajo nuestra supervisión.

PhD. Esteban Alejandro Valencia Torres	**DSc. Víctor Hugo Hidalgo Díaz**
DIRECTOR PROYECTO	**CODIRECTOR PROYECTO**

ACKNOWLEDGEMENT

Special thanks to the Lord for the intelligence, and ability.
To my beloved family, and Carolina for the support, care, and love.
To the LMH Lab's *family*, and colleagues for their friendship, and patience, and
to the research team for sharing their knowledge, and expertise.

To the **Lord**,

"…who is the first and the last, the beginning and the end, the time and the eternity…"

TABLE OF CONTENTS

TABLE OF FIGURES

LIST OF TABLES

SUMMARY

During the last decade UAVs have contributed to a fast pace of innovation in different areas such as: agriculture, delivery, surveillance, post disaster-assessment, among others. The aircraft design process for these platforms present less constrains, since they are unmanned systems, and usually require less investment than other aviation sectors. Those aspects require a versatile, and good enough method for preliminary design to define UAV weight and performance. In this context, the present work defines a parametric methodology, which couples several aircraft design tools to assess the performance of UAVs in the Andean Region. The developed modules have been focused on weight, aerodynamic, and mission performance. Parametric tools given in the open domain have been adapted and refined to study UAVs ranging from Small to High Altitude Long Endurance, where the use of common aircraft design codes fail to capture trends in their performance. Results from weight sensitivity analysis showed that geometric, and aerodynamic variables are useful to reduce the takeoff total gross weight, and improve the overall UAV performance.

Keywords: Aircraft Preliminary Design, UAV Performance, UAV Weight, UAV Sizing, Performance Assessment, SUAS, and HALE UAV.

GLOSSARY

A	Aspect Ratio
AC	Adapted Camera
C_D	Drag Coefficient
C_L	Lift Coefficient
C_P	Power Coefficient
C_{DO}	Zero Lift-Drag Coefficient
CFD	Computational Fluid Dynamics
D	Drag
e	Oswald's Efficiency Factor
E	Endurance
E_{Esp}	Specific Energy
EPS	Electrical Propulsion System
ESC	Electronic Speed Controller
f_{Usable}	Battery Depth of Discharge
H	Operating Altitude
H_{th}	Theoretical Altitude
HALE	High Altitude Long Endurance
h_t	Horizontal Distance Covered in the Airborne Phase
J	Advance Ratio
k	Induced Drag Factor
L	Lift
MSC	Multispectral Camera
MF_{Batt}	Battery Mass Fraction
P_A	Power Available
P_R	Power Required
P_{Max}	Maximum Power
PA	Precision Agriculture
PWM	Propulsion Weight Module
P_{Py}	Power Required by Payload
R	Range
RC	Rate of Climb

R_c	Radius of Curvature
S_w	Wing Planform Area
S_g	Ground Run Distance
SWM	Structural Weight Module
SSM	Site Specific Management
SUAS	Small Unmanned Aerial System
T	Thrust
TIU	Thermal Imaging Unit
UAV	Unmanned Aerial Vehicle
UAS	Unmanned Aerial System
WTO	Takeoff Total Gross Weight

Δ_{PPW}	Percentage Change in Power Plant Weight
Δ_{SW}	Percentage Change in Structural Weight

ρ	Density
η	Efficiency
γ	Flight Path Angle
μ_r	Friction Coefficient
σ	Ultimate Load Factor

INTRODUCTION

I. Research Question

How can be assessed the interaction between weight and performance of electric-powered unmanned aerial vehicles in the Andean Region?

II. General Objective

To develop a parametric model to assess the weight and performance of electric-powered unmanned aerial vehicles in the Andean Region

III. Specific Objectives

- To develop parametric models to study the weight and performance of electric-powered UAVs operated in the Andean Region.
- Preliminary design of structure, power plant, and fixed equipment parameters to feed the weight module of electric-powered UAVs.
- To assess the performance of electric-powered UAVs in different mission stages under the Andean Region operating conditions.

IV. Scope

The present work developed a parametric model based on the analytical approach to assess the weight and performance of electric-powered UAV ranging from Small (SUAS) to High Altitude Long Endurance (HALE) Unmanned Aerial Systems. These aerial systems are focused on the application of precision agriculture techniques in the Andean Region. *Weight estimation* considers structural, power plant, and fixed equipment components, and *Performance Study carries* out range, endurance, and energy consumption specifications for different mission stages. The weight and performance validation at cruise condition is based on a low-cost UAV focused on research activities, and the mission stage evaluation uses an electric-powered aircraft developed at Politecnico di Milano validated with experimental methods.

1. THEORETICAL FRAMEWORK

1.1. UAV Performance Assessment

The aircraft performance has a direct relation with operating conditions and mission profile [1], hence the performance analysis assumes weight, power plant, geometric, aerodynamic, and operating flight characteristics. Flight performance is studied under two methods: the analytical and the numerical [2]. The analytical method simplifies the Drag Coefficient (C_D) using semi-empirical methods based on geometric parameters and flow conditions. On the other hand, the numerical method needs an aerodynamic characterization from experimental assessments or computational simulations [3].

The performance assessment involves different criteria depending on the author. A traditional aircraft performance analysis involves weight, propulsion, and aerodynamic characteristics to relate operating conditions and preliminary aircraft design with energy consumption. Performance methodologies involve different design stages such as: preliminary design, energy consumption, evaluation, and optimization. Kontogiannis [4] supports the design stage on weight estimation models and geometric parameters, it mentions the performance and optimization evaluation are based on drag coefficients calculations, propulsion system, stability, control, and aerodynamic analysis with CFD support. Avanzini [5] developed a methodology based on battery-powered aircraft focuses on the battery model and performance optimization in terms of electric variables related with battery's material and UAV operating conditions. Cinar [6] proposed a new approach to study the influence of aircraft subsystems in the case of unconventional designs that cannot be fully capture by empirical relationships, encouraging the analysis of subsystems influence on general energy distribution, based on a multidisciplinary analysis that consists on weights, propulsion, and aerodynamics, all these to obtain a detailed analysis of requirements [7].

Kontogiannis' research is focused on conceptual and preliminary aircraft design for light, electric-powered UAV [4]. Conceptual design involves aircraft data, operating conditions, and weight estimation process. Preliminary design determines the perfect combination between wing lift coefficient, planform area, and aerodynamic surface

based on drag coefficient calculations, propulsion system analysis, aircraft performance, stability, and flight characteristics. The advantages of using this work is the way in which is implemented the weight, performance, and optimization process into one assessment methodology, and the use of CFD analysis to achieve aerodynamic characterization, due to lack of wind tunnel facility. On the other hand, a limitation of this work is the use of micro UAV with an approximate WTO of 2 [kg], and low speeds around 12 [m/s].

Avanzini developed a battery model in which is considered the optimal performance and sizing of small fixed wing electrically-driven propeller UAVs [5]. The discharge model considers constant discharge current, and constant battery voltage in which time is a direct function of discharge capacity, and absorbed power. Avanzini's model does not use as input the voltage variation, due to current and residual capacity. Hence, it does not need numerical discretization to use Peukert models [8]. Furthermore, a battery sizing model is proposed to optimize the endurance and range based on the constant-power discharge model. In which, best airspeed values are obtained based on battery characteristics.

Cinar established an alternative methodology to assess the relation between size, and novel propulsion technologies [6]. A traditional way to evaluate the aircraft sizing and performance is to relate weight, propulsion, and aerodynamics. Nevertheless, Cinar considers two distinguishable design considerations based on: aircraft design and equipment due to mission requirements, and unconventional propulsion systems such as: hybrid-electric, and electric systems. The propulsion methodology was developed for electric motors paired with LiPo batteries in small UAVs.

The present work develops parametric models based on the analytical approach to evaluate the influence of WTO in UAV performance. For this purpose, a sensitivity analysis of the WTO components based on structural, power plant, and fixed equipment is carried out. The chosen case of study is an UAV with a conventional airframe implemented for PA in the Andean Region. The contribution of this study is the development of a methodology for an electric-powered, low cost UAV used for monitoring, which is important as most of the studies regarding UAVs have focused on

military applications, and hence, their budget is larger than SSM applications [9]. Furthermore, the present work enables the identification of key weight contributors to WTO and hence allows the assessment of optimal configurations for PA.

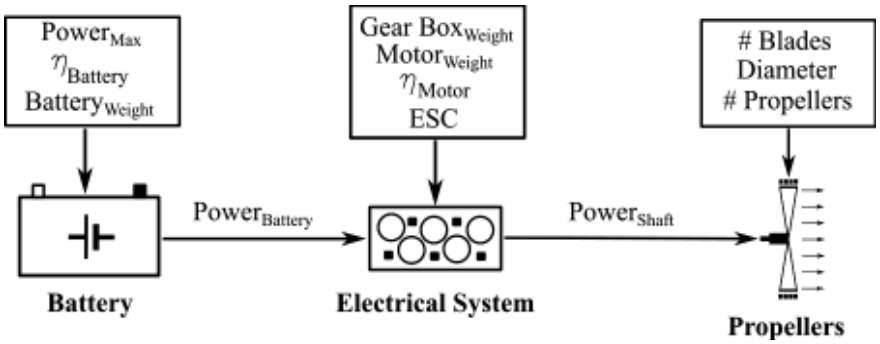

Figure 1.1. Energy system.

Figure 1.2. represents the power plant energy system, in which the energy source is a battery capable of providing enough energy to generate the movement of an electric motor that drives a propeller. This energy transformation process considers the exchange of chemical energy into mechanical energy using electronic instruments, and support mechanical mechanisms, which present efficiencies increasing the power demand from the battery.

1.3.1. Performance Model

The performance model has been developed for the UAV at steady symmetrical and non-accelerating flight [10].

$$E = \frac{E_{Spec}}{g} * MF_{Batt} * \prod\eta * \eta_{Batt} * f_{Usable} * \frac{L/D}{V} \quad (1.1.)$$

$$R = \frac{E_{Spec}}{g} * MF_{Batt} * \prod\eta * \eta_{Batt} * f_{Usable} * \frac{L}{D} \quad (1.2.)$$

Equation 1.8 and Equation 1.9 represent the Breguet and the Range equation, respectively, applied for electric-powered unmanned aircraft platforms. These equations involve material, thermodynamic, aerodynamic, and flight operating

characteristics. The accounted variables for endurance and range calculation are battery's specific energy (E_{Spec}), battery mass fraction (MF_{Batt}), electrical system efficiency $\prod\eta$, permisible battery pack depth of discharge (ratio between battery usable energy, and total stored energy) (f_{Usable}), aerodynamic forces ratio (L/D), and flight velocity (V) [11].

1.3.2. Mission Profile Stages of Flight.

Mission profile is composed of different mission segments in which is intended to achieve an objective. Each one of these segments has specific energy considerations, and requirements in terms of speed [11].

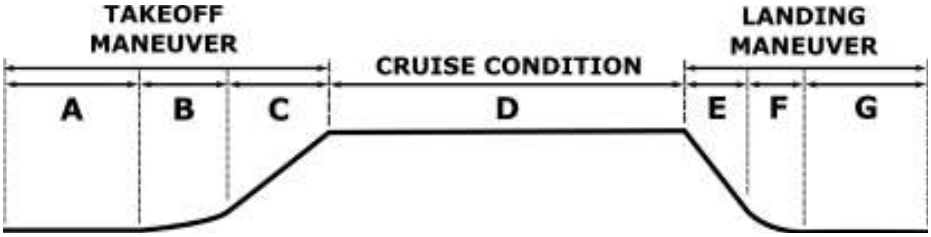

Figure 1.2. Multiple mission profiles [11].

Figure 1.2. shows the entire mission profile, and the mission segments. The *Takeoff Maneuver* is composed of Ground Run Distance (**A**), Airborne Distance (**B**), and Climb (**C**). The *Cruise Condition* (**D**) is the longest mission segment. The *Landing Maneuver* is composed of Descent (**E**), Airborne Distance (**F**), and Ground Run (**G**). The following sections describe in

1.3.3. UAV Weight Estimation Module

Preliminary weight estimation models have several years of development, due to its influence on aircraft design and performance. Weight prediction has a direct relation with preliminary design stage, project stage, flight stage, and research [12]. Preliminary design stage is the phase in which a new UAS is conceived, hence the Unmanned Aerial Vehicle (UAV) size, propulsion architecture, mission profile, and flight performance are established. Project stage determines the aircraft production based on design requirements, considering higher levels in performance and payload

capabilities to produce competitive UAS. Flight stage considers the performance and influence of weight during flight and its effects on aircraft stability. Weight research studies the effect of design decisions, hence materials, methods, and techniques are analyzed in order to improve the current situation and achieve better results with less resources consumption.

$$WTO = \frac{W_{Payload} + W_{Instrumentation} + W_{Electrical\,System}}{1 - \left(MF_{Strct} + MF_{Power\,Plant} + MF_{Fixed\,Equipment}\right)} \qquad (1.3.)$$

Equation 1.10. is the sizing equation used to estimate the WTO. Sizing equation has powerful implications because of its accuracy, and robust in different UAVs' weight estimation [11]. The following paragraphs slightly describe the components, and their parameters of influence in the estimating process. It is based on Valencia's research [13].

Through the past of the years, several authors have developed methodologies to estimate the aircraft Takeoff Total Gross Weight (WTO) based on aircraft capabilities, size, and mission approaches. However, the preliminary design process is improved by aerodynamic optimization, material selection, propulsion architecture design, and payload configuration. The following paragraphs study several methodologies developed in different periods of time by Roskam [14], Zhang [15], and Pornet [16] to identify their positive influence, and limitans. Roskam [14] presents a methodology for estimating airplane's components weight based on mass fraction method. Zhang's [15] uses statistical data combined with numerical analysis to establish formulas to estimate structural weight in UAS. Pornet [16] introduces the hybrid concept on preliminary aircraft design with the development of a methodology to assess the size and performance of UAVs using a hybrid electrical-combustion thermodynamic cycle.

Roskam's airplane design method is supported by statistical data to estimate the weight component[14]. This methodology is based on aircraft size and mission approach. The available estimating methods are: Cessna Method for small, relatively low performance type airplanes with maximum speeds below 200 [kts], USAF Method for light and utility type airplanes with performance up to about 300 [kts], General

Dynamic method for propeller-driven small aircraft, and the Torenbeek method for transport airplanes and business jets with design dive speeds above 250 [kts]. An advantage of Roskam's method is its versatility because the WTO is divided into three components established such as: structural, power plant, and fixed equipment weight, and a disadvantage of this method is the accuracy, and applicability of several correlations for UAVs.

Zhang developed a methodology based on linear regression methods to assess the structure weight of HALE UAVs, and carry out a sensitivity analysis for preliminary aircraft design process [15]. The study considers: wings, V-Tail, fuselage, and landing gear weight components. An advantage of Zhang's research is the independent analysis of aircraft structural components based on statistical data of the overall parameters which have influence on UAV structure weight. On the other hand, a disadvantage of this method is the use of specific materials to establish wing and fuselage correlations.

Pornet's research makes contrast between fuel-energy and hybrid-energy aircraft in terms of size and performance [16]. To this purpose was developed a methodology in which electric and mechanic components are involved with their efficiencies, weights, and influence over the whole system. The contribution of this methodology is the electrical system approach. Nevertheless, in the future it could be useful to propose hybrid models.

This research is focused on the estimation of WTO for an Electric powered UAV used for PA in the Andean Region. For this, the models previously discuss have been integrated in a WTO module to carry out a sensitivity analysis, and identify the optimization aspects to improve the overall system. The importance of an accurate weight prediction tool lies on the direct relation of this parameter into the preliminary aircraft size and performance characteristics. Preliminary weight estimation models have several years of development, due to its influence in aircraft performance. The categorization is based on aircraft capabilities, aircraft sizing, and mission approaches. The models presented by Roskam [14] have the fundamentals of aircraft preliminary design, but these methods are old and its applicability is limited for UAVs because of

the considerations based on aircraft categories, and mission approaches. Zhang's [15] is practical as it uses statistical data combined with numerical analysis, to establish formulas unmanned aerial systems, however, this method only considers the structural weight. Pornet [16] introduces the hybrid concept on preliminary aircraft design with the development of a methodology to assess the size and performance of UAVs, using a hybrid electrical-combustion thermodynamic cycle.

2. METHODOLOGY

This section describes a parametric methodology for weight and performance assessment of UAS. For this task, current models for weight and performance, implemented in civil, [14] aviation have been adapted and defined [11]. The present methodology has been developed to encompass SUAS to HALE aerial systems. Figure 2.1. shows the general assessment methodology implemented to calculate aircraft performance. In this figure, the operating conditions, and aircraft data modules define the flight height, flight Mach number, airframe, geometric, and propulsive characteristics. The weight module establishes a preliminary WTO to feed the performance and energy source module in which is defined the energy consumption for cruise.

The aircraft data feeds the weight module regarding the airframe, geometric, and propulsion aspects. The weight module is related to the performance and energy source module by WTO and battery's specific Energy. Regarding the propulsion system, it has been selected a baseline concept with tube-wing configuration and one electric-powered propeller. The energy source system comprises: battery, power plant, and electrical system.

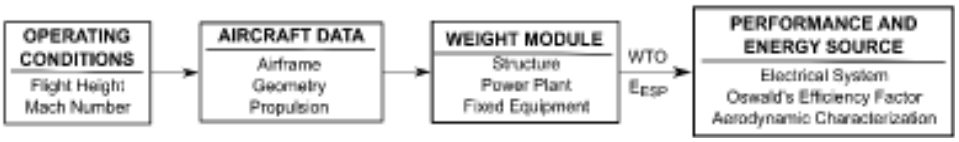

Figure 2.1. General assessment methodology.

2.1. Performance and Energy Source Module

The performance module determines the energy consumption based on battery’s type, and operational requirement features. For this effect, the methodology presented in Figure 2.2. is implemented to study the overall UAV performance.

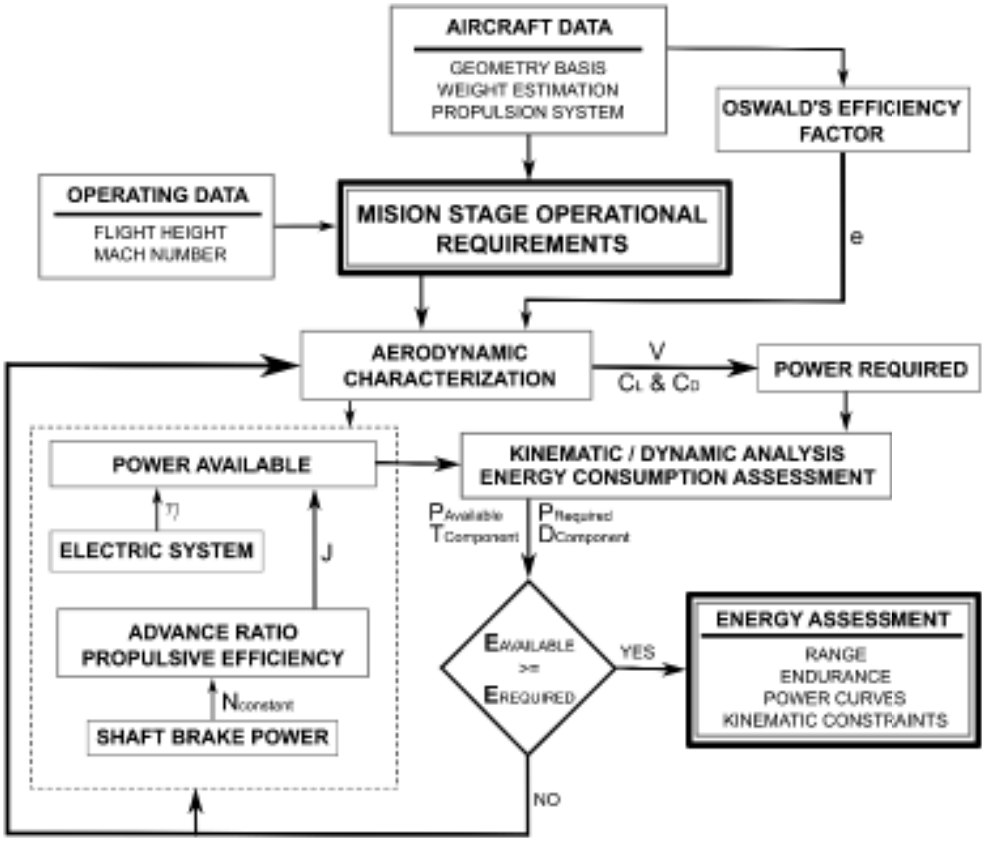

Figure 2.2. Performance and energy source module.

Figure 2.2. the calculation process implemented in the Performance and energy source module is described. As observed, the inputs required for this module are operating conditions and aircraft data, which then, feed the Oswald's Efficiency Factor (e) algorithm, which calculates e as function of the aircraft geometrical data. This latter parameter defines the lift deterioration, and hence, enables the calculation of Drag polar and Power Required (PR). On the other hand, the energy source module determines the energy available based on electric-powered system characteristics (Power Available PA). Once, PA and PR are estimated, the energy consumption at mission stage operational requirement can be calculated, and compared to stablish the UAV energy assessment.

2.1.1. Mission Stages: Performance Assessment

This section shows the performance methodology to assess the range, endurance, and energy consumption of an UAV in high altitude regions.

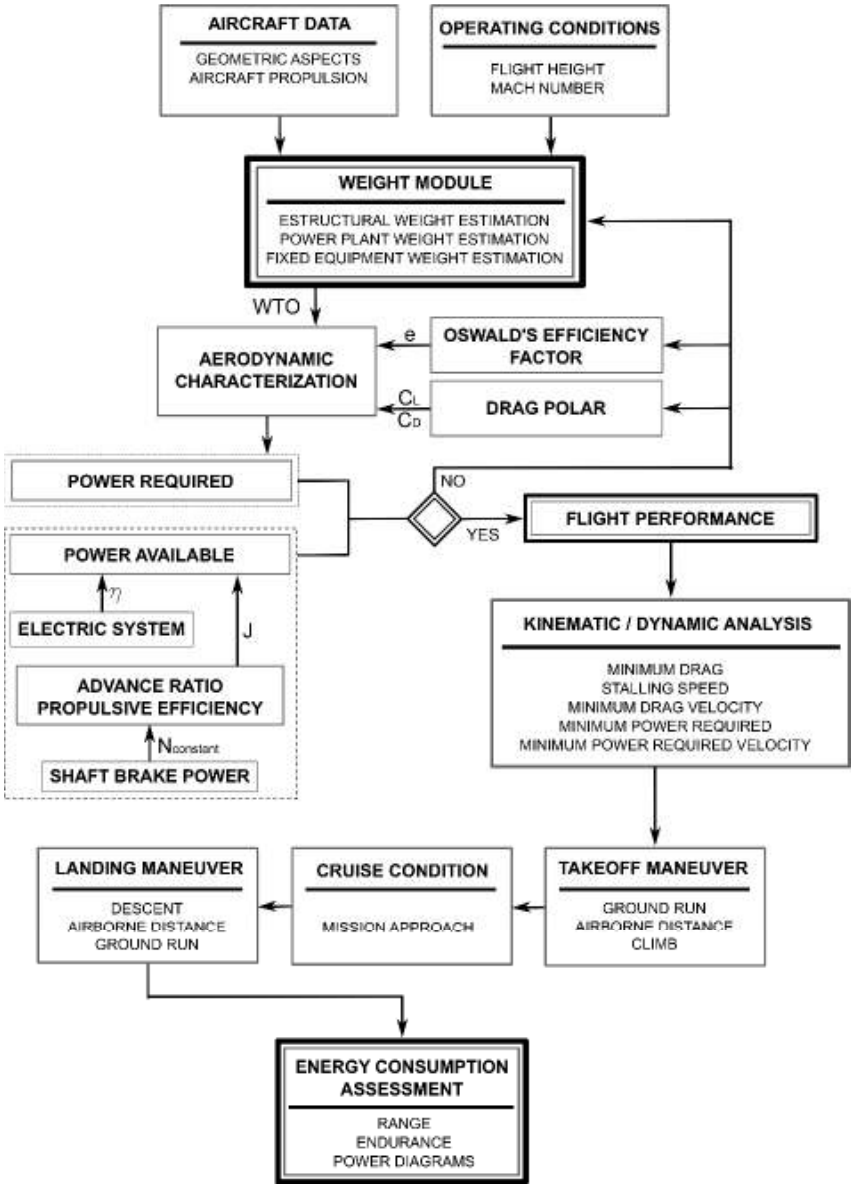

Figure 2.3. Methodology for performance assessment.

Figure 2.3. shows the implemented methodology to assess the energy consumption, and UAV capabilities. The operating conditions, and aircraft data feed simultaneously the weight and the aerodynamic characterization modules. Then a power assessment

based on energy system, and power plant capabilities is realized to start the performance assessment per mission stage. For this purpose, the mission is divided into three stages denominated: takeoff maneuver, climb, cruise, descent, and landing maneuver. Each one of these stages has kinematic parameters, and energy considerations as will be shown in the following paragraphs.

2.1.1.1. Takeoff Maneuver

Takeoff maneuver is divided into three stages: ground run distance, transition distance or airborne distance, and climbout. Figure 2.4. represents each stage, with the specific conditions based on airworthiness requirements.

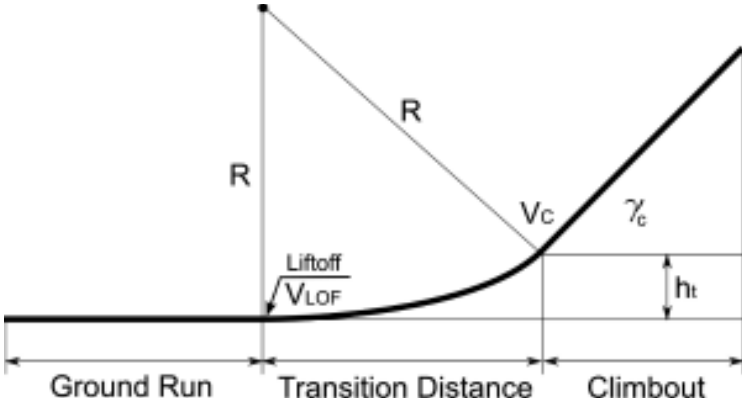

Figure 2.4. Schematic for takeoff maneuver [10].

The ground run distance involves motion and kinematic equations to study the aircraft performance at takeoff maneuver. The assumptions consider in this part are: horizontal runway, no wind, constant weight, and angle of attack equal to zero (T // V). Airborne phase considers the transition flare distance in which engine control setting is constant, and the airplane leaves the ground until it reaches the steady climb altitude. The takeoff flight path is reached when the airplane overcomes the airport's screen height, and it starts the climbout stage [10]. The following equations, from 2.1 to 2.6, define the UAV takeoff maneuver in terms of ground run distance, mean acceleration, thrust required, airborne path radius, path angle, and airborne horizontal distance, respectively [10].

$$S_g = \frac{W/Sw}{\rho * g * (C_{Dg} - \mu_r * C_{Lg})} \ln\left[\frac{\frac{T}{W} - \mu_r}{\frac{T}{W} - \mu_r - \frac{C_{dg} - \mu_r * C_{Lg}}{(C_L)_{LOF}}}\right] \quad (2.1.)$$

$$\bar{a} = \frac{V_{LOF}^2}{2 * S_g} \quad (2.2.)$$

$$T = \left[\frac{\bar{a}}{g} + \mu_r + \left(C_{Dg} - \mu_r * C_{Lg}\right) * \frac{\frac{1}{2} * \rho * V_{(0.7*V_{LOF})}}{\frac{W}{S}}\right] * W \quad (2.3.)$$

$$R = \frac{V_{LOF}^2}{g * (\sigma_{LOF} - 1)} \quad (2.4.)$$

$$\gamma_s = \left(\frac{2 * H_s}{R}\right)^{\frac{1}{2}} \quad (2.5.)$$

$$S_a = R * \gamma_s = \frac{V_{LOF}^2}{g * (\sigma_{LOF} * 1)} * \left(\frac{2 * H_s}{R}\right)^{\frac{1}{2}} \quad (2.6.)$$

In kinematic terms, velocities applied for takeoff maneuver considers: minimum control velocity (V_{MC}), rotation speed (V_R), Liftoff Velocity (V_{LOF}), minimum liftoff velocity (V_{MU}), and climbout velocity (V_{CL}). The latter terms have a common pivot, the minimum stalling speed (V_S). Hence, the assumptions in terms of velocity for this study are: $V_S = V_{MC}$, $V_{CL} = 1.2 * V_S$, $V_{LOF} = V_{ROC_{MAX}}$, $V_{MU} = V_{LOF}$ / 1.1, and the assumptions in terms of external agents are: rolling friction (μ_r) equal to 0.02 for concrete or 0.05 for cut grass, and mean thrust value taken from a typical variation of Thrust with Mach Number Curves [10].

2.1.1.2. Symmetric Climb

Climb condition is the phase in which the aircraft started the climbout until reach the flight height. Three performance values are important in climb: time required to climb, horizontal distance covered during climb, and amount of energy consumed during climb [1, 9]. The parameters that defines the climb operation are: maximum rate of

climb, rate of climb at steady flight, minimum climbing time, airspeed for maximum rate of climb, and maximum climb angle. The latter are represented in the following equations, from 2.7 to 2.11.

$$RC_{Max} = \frac{P_a}{W} * \sqrt{\frac{2 * W}{Sw * \rho * (C_L^3/C_D^2)_{Max}}} \quad (2.7.)$$

$$RC_{SF} = \frac{T * V - D * V}{W} \quad (2.8.)$$

$$t_{min} = \frac{(H_{th} - H)}{RC_{Max}} \ln\left[\frac{1}{1 - \frac{H}{H_{th}}}\right] \quad (2.9.)$$

$$V_{e_{RC\,Max}} = \sqrt{\frac{2 * W}{Sw * \rho_0 * (C_L)_{(C_L^3/C_D^2)Max}}} \quad (2.10.)$$

$$\sin(\gamma_{Max}) = \frac{T}{W} * \left(\frac{1}{(C_L/C_D)_{Max}}\right) \quad (2.11.)$$

The Rate of Climb (ROC) at steady flight considers the excess power available in the energy source. The effects of wind in climb are neglected in this study.

2.1.1.3. Cruise Condition

Cruise condition is the most important mission segment in terms of energy consumption [11]. Hence, the major goal is to define performance parameters to achieve the minimum energy consumption, in order to maximize the UAV endurance, and range. Cruise considers that $Lift = Weight$, hence the aerodynamic characterization is achieved with Lift-Drag Parabolic Approximation [17], energy consumption requirements are based on electric-powered Breguet equation, and range [10] is defined as a variant of Breguet's Equation.

$$V_{D_{min}} = \sqrt{\frac{2 * W}{Sw * \rho * \sqrt{C_{Do} * \pi * A * e}}} \quad (2.12.)$$

$$V_{P_{r_{min}}} = \sqrt{\frac{2 * W}{Sw * \rho * \sqrt{3 * C_{Do} * \pi * A * e}}} \quad (2.13.)$$

$$V = \sqrt{\frac{2 * W}{Sw * \rho * C_L}} \quad (2.14.)$$

$$D_{min} = \left[C_{Do} * \frac{1}{2} * \rho * V_{D_{min}}^2 * Sw\right] + \left[\frac{W^2}{\pi * A * e * \frac{1}{2} * \rho * V_{D_{min}}^2 * Sw}\right] \quad (2.15.)$$

$$P_{r_{min}} = \frac{4}{3} * W * \sqrt{\frac{2 * W}{Sw * \rho} * \sqrt{\frac{3 * C_{Do}}{(\pi * A * e)^3}}} \quad (2.16.)$$

The latter formulas, from 2.12 to 2.16, define the UAV optimal kinematic parameters. These equations relate aerodynamic data, operating conditions, and aircraft configuration with energy consumption. The evaluation, and management of these preliminary design parameters establish the aircraft's design space in terms of airspeed, and power requirements.

2.1.1.4. Symmetric Descent & Airborne Distance

In the descent phase the aircraft reduces its velocity to a certain value called Steady Approach Speed that enables the landing. The airborne distance for landing is composed of two parts: the final approach, and the transition distance. The final approach considers the screen location, and the transition distance is related with the aircraft's touchdown [1, 21]. The following equations, from 2.17 to 2.19, represent the angle of descent, the flare's radius of curvature, and the horizontal distance covered by the airborne distance, respectively.

$$\gamma_{dA} = \sin^{-1}\left[\frac{C_D}{C_L}\right]_A \tag{2.17.}$$

$$R = \frac{V_A^2}{g * (\sigma_A - 1)} \tag{2.18.}$$

$$h_t = \frac{1}{2} * S_t * \left[\gamma_{dA} + \left[\frac{C_D}{C_L}\right]_T\right] + \frac{V_A^2 - V_T^2}{2 * g} \tag{2.19.}$$

For this section, the assumption made by Riboldi [19] and Ruijgrock [10] in terms of velocity is represented by $V_A = 1.3 * V_S$. In which, V_A is the approach velocity, and V_S is the stalling speed. Furthermore, for touchdown the drag and lift coefficient need to be estimated at $1.15 * V_S$.

2.1.1.5. Landing Maneuver

Figure 2.5. represents the mission segments involved in landing maneuver. These segments are represented by: final approach distance, transition or airborne distance, and ground run distance.

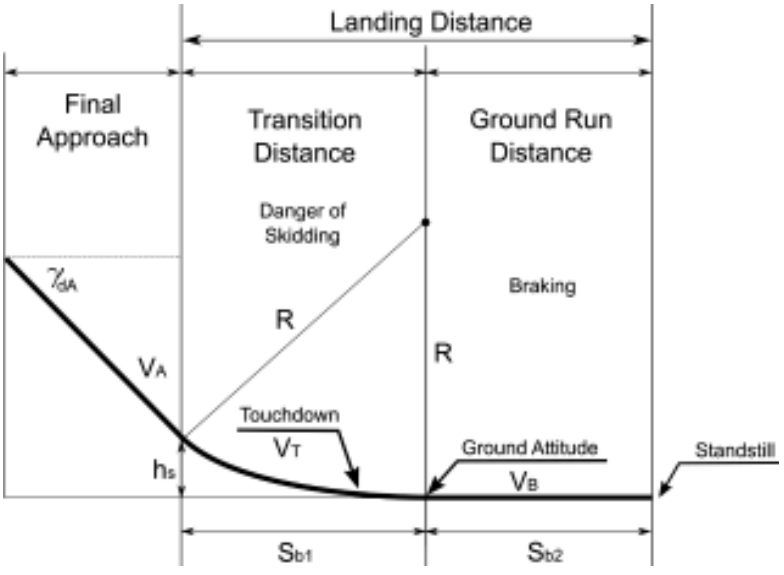

Figure 2.5. Schematic for landing maneuver [10].

The landing ground run starts after touchdown. In this phase, the airplane has two different stages. The first one is the skidding distance between touchdown velocity V_T and brake velocity V_B, and the second is the maximum braking distance in which the aircraft will be completely stopped [10]. To define this stage is important the identification of different parameters such as: acceleration, brake velocity, danger of skidding distance, and maximum braking distance, as is shown from equation 2.20 to equation 2.23.

$$\frac{dV}{dt} = \frac{g}{W} * [-C_{Dg} * \frac{1}{2} * \rho * V_B^2 * Sw - D_{g_{Max}}] \tag{2.20.}$$

$$V_B = \sqrt{\frac{W - \frac{D_{g_{Max}}}{\mu_B}}{C_{L_g} * \frac{1}{2} * \rho * S_w}} \tag{2.21.}$$

$$s_{b_1} = \frac{V_T^2}{2 * g * \mu_b * Z} \ln\left[\frac{1+Z}{1+Z\left(\frac{V_B^2}{V_T^2}\right)}\right] \tag{2.22.}$$

$$s_{b_2} = \frac{W}{C_{D_g} * \rho * g * Sw} \ln\left[\frac{C_{D_g} * \frac{1}{2} * \rho * V_B^2 * S_w}{D_{g_{Max}}} + 1\right] \tag{2.23.}$$

The horizontal distance covered in the landing is composed of two parts (s_{b_1} & s_{b_2}). The first distance is denominated as danger of skidding distance, and the second is the maximum braking distance. Both generates the landing ground run.

2.1.2. Aerodynamic Model

In this work, a simple aerodynamic characterization is implemented, in order to calculate the drag polar, based on the aircraft geometrical aspects. The following paragraphs describe the method used to obtain the aircraft aerodynamic characterization [20].

2.1.2.1. Oswald's Efficiency Factor

Oswald's Efficiency Factor (e) refers to the aerodynamic efficiency for parabolic lift-drag polar. Oswald factor reflects the lifting properties deterioration, due to elliptical lift distribution distortion, produced by interference effects, caused by the angle of attack, and the increase of drag components [21]. The present work has implemented a parametric model based on Samoylovitch [21], to determinate the Oswald's efficiency factor, at preliminary design stages, due to geometric aspects.

$$e = e_w * k_F = \frac{(e_{w/S_c} = 1) * (e_{w/S_c} = 0)}{(S_c * e_{w/S_c} = 0) - (1 - S_c) * (e_{w/S_c} = 1)} * k_F \qquad (2.24.)$$

Equation 2.24 represents the determination of *e* due to lifting properties deterioration in a representative shape. Where, e_w denotes the relation between the wing circulation distribution and an elliptical one, with and without the influence of the leading-edge suction force. $e_{w/S_c} = 1$ represents the implementation of leading edge suction force, $e_{w/S_c} = 0$ is the zero-leading edge suction force, S_c is the relative leading-edge suction force, and k_F represents the section shape factor based on wing span and fuselage measures.

2.1.2.2. Drag Calculation

Drag Polar calculation has different estimation methods to satisfy engineering calculation regarding. These methods consider mathematical formulations, CFD simulation, and experimental data. First, semi-empirical method and the semi-empirical method calibrated by previous experience are mathematical methods based on basic geometric parameters, flow conditions, and historical data from similar configuration aircraft that generates an appropriated numerical correction. Next, CFD simulations encourages to design high lift devices with $C_{L_{MAX}}$ and $C_{D_{min}}$, but CFD need support of semi-empirical methods to calculate the wave drag, and increases the aircraft preliminary design process. Moreover, wind tunnel data experiments are used to confirm and guarantee the performance of mandatory requirements in the conceptual phase.

The drag polar method used for developing the current work is a semi-empirical method based on a mathematical formulation of two-term approximation which is represented in Equation 2.25. At this stage, this simple approach has been implemented for the aircraft drag calculation. C_{Do} is the zero-lift drag coefficient, and A represents the aspect ratio. Furthermore, for the lift calculation at cruise condition, it has been assumed a flight condition of steady, symmetrical, and non-accelerated flight.

$$C_D = C_{Do} + C_{DL} = C_{Do} + (k * C_L^2) = C_{Do} + \frac{C_L^2}{\pi * A * e} \quad (2.25.)$$

2.1.3. Energy Consumption Assessment

Performance relates energy requirements with UAV endurance, range, and capability. A simple method to estimate a power balance is defined by Ruijgrock [10] as follows:

$$\begin{gathered} T - D - W * \sin(\gamma) = 0 \\ (T * V) - (D * V) - W * (\sin(\gamma) * V) = 0 \\ P_A = P_R + W * RC \end{gathered} \quad (2.26.)$$

The present work establishes the energy consumption of an electric UAV at cruise condition, considering that lift is equal to weight, and with this, it is calculated the velocity for maximum endurance.

2.1.3.1. Power Required

Based on Avanzini's research, the power required for an UAV is composed of three different components [5]: energy consumed by avionics, payload, and the power required to accomplish the mission, as is shown in Equation 2.27.

$$P_{Req.Total} = P_{Avionics} + P_{Payload} + P_{Required} \quad (2.27.)$$

Considering the baseline information exposed about energy consumption, the term P_{Req} in Equation 2.26 can be replaced by the term $(D * V)$ as was demonstrated. In this way, the application of the aerodynamic characterization established by drag polar, and Oswald's Efficiency Factor can be introduced to power required study as is shown.

$$P_{Req.Total} = P_A + P_{Py} + P_R = P_A + P_{pl} + W * \sqrt{\frac{2 * W * C_D^2}{3 * \rho * C_L^3}} \qquad (2.28.)$$

Equation 2.28 shows the influence of aerodynamic coefficients, mission approach, weight, and preliminary design of UAVs in the calculation of $P_{Req.Total}$. Hence, in the aerodynamic side the estimation of C_L an C_D and the relation with e are important considerations to remark. While, in the preliminary design stage the remarkable topics are operating conditions, aircraft data, and weight estimation.

2.1.3.2. Power Available

Equation 2.29 was utilized to calculate the power available, which is based on electric source, power coefficient, advance ratio, and propulsive efficiency. At this stage, two assumptions were made to estimate P_A. Firstly, it was considered that the electric energy system is composed of battery, electronic speed controller, and transmission mechanism with independent efficiencies [16]. Secondly, the power coefficient C_P satisfies the condition of equal magnitude between power shaft brake PSB and propulsive power P_P. In equation 2.29 the advanced ratio (J), was used to relate the aircraft velocity, engine speed, and propeller's diameter, whilst the propulsive efficiency (n_p) was implemented to relate thrust coefficient (C_T) with power coefficient and advance ratio. For this preliminary design to define power coefficient and advance ratio was used Roskam's Propeller Chart [14].

$$P_A = \frac{C_T}{C_P} * \frac{V}{n_p * D} * V * I * \eta_{Batt} * \eta_{ESC} * \eta_{PI} \qquad (2.29.)$$

2.2. Weight Modelling

WTO considers structural, power plant, and fixed equipment components. Within each component there are several subsystems, which need to be identified and modelled to define all the design space variables for weight. For instance, the structural component comprises wings, empennage, fuselage and landing gear [15].

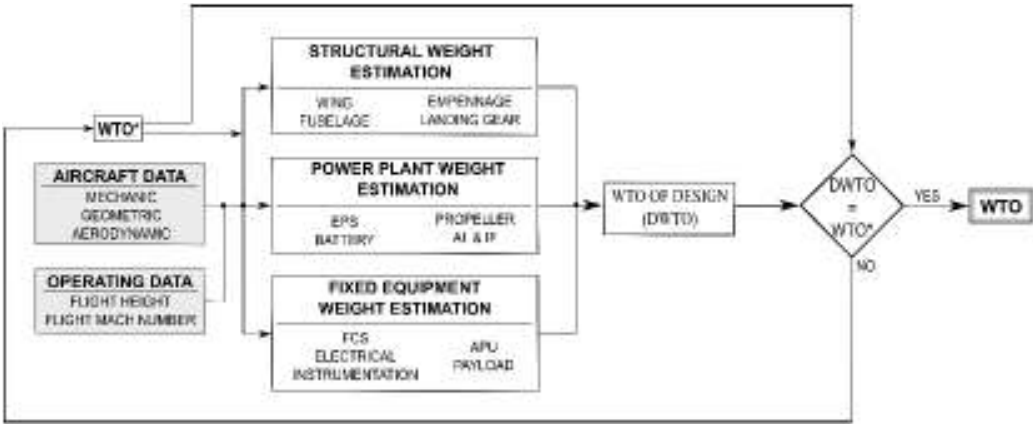

Figure 2.6. Weight modelling methodology.

Figure 2.4. shows the implemented methodology to estimate WTO. As mentioned previously, the operating condition, and aircraft data module, feed the weight module. Since some components require the WTO to estimate their weight, an iterative calculation was implemented. For this purpose, the design total gross weight (DTWO) was defined when the guessed total gross weight (WTO*) matched the calculated WTO.

2.2.1. Structural Weight Estimation

Equation 2.30 shows the parameters to analyze the structural weight [11]. In the next paragraphs is further described each subsystem in this component.

$$W_{Struct} = W_{Wing} + W_{Emp} + W_{Fuse} + W_{LG} \tag{2.30.}$$

2.2.1.1. Wing Weight Estimation

Wing weight estimation is an important subsystem in the structural weight calculation, due to its influence in the aerodynamical performance, and hence the overall system efficiency. Many authors have developed correlations based on statistical analysis taking in consideration material resistance, geometrical aspects, and aerodynamic characteristics. Equation 2.31 shows Roskam's [14] correlation based on the Cessna method, for cantilever wings, and Equation 2.32 shows Chun's [12] correlation for moderate performance light utility aircraft.

$$W_{wing-R} = 0.04674 * (WTO)^{0.397} * S_w^{0.143*\sigma*0.397} * A^{1.712} \quad (2.31.)$$

$$W_{wing-C} = 96.948 * \left[\left(\frac{WTO * \sigma}{10^5}\right)^{0.65} * \left(\frac{AR}{\cos(\Lambda)_{1/4}}\right)^{0.57} * \left(\frac{s_w}{100}\right)^{0.61} * \left(\frac{1+\lambda}{2*\left(\frac{t}{c}\right)}\right)^{0.36} * \left(1+\frac{V_e}{500}\right)^{0.5}\right]^{0.993} \quad (2.32.)$$

Since Chun's correlation predicts wing weight for light aircraft with good accuracy (2-5%), this approach has been selected for the present work. Nevertheless, latter equation presents the issue that design ultimate load factor σ is not defined at this early stage of design [12], to tackle this problem Equation 2.32 has been used to calculate σ and to solve this second equation the wing weight is assumed equal to 0.1*WTO.

2.2.1.2. Empennage Weight Estimation

The empennage correlation given by Gundlach [11] is used for this study. Equation 2.33 relates two parameters: the aerial weight of the tails (WA_{Emp})and the empennage area (S_{Emp}). The first parameter represents an average weight for tails per square meter, and it has different values due to material. For instance, composite [11] material's a suggested value is around 2.44 [kg/m2].

$$W_{Emp} = WA_{Emp} * S_{Emp} \quad (2.33.)$$

2.2.1.3. Fuselage Weight Estimation

Commonly, the fuselage of manned aircraft is made with aluminum alloys. However, the fuselage for UAVs for PA has different treatments in the manufacturing processes, since in PA application low weight and cost are main drivers. In most of the cases, the fuselage is the biggest part of an aircraft, and hence, it is an important component in the WTO optimization process [18]. Yi Zhang [15] develops a correlation to be used for large fuselage fineness ratio, considering a fuselage made of aluminum alloy material. Yi Zhang [15] relates five parameters such as: air intake pattern (K_{inlet}), dynamic pressure (q), total gross weight (WTO), fuselage structure length (L), and fuselage structure height (H) to establish a preliminary fuselage weight, as is shown in Equation 2.34.

$$W_{Fuse} = 0.0025 * k_{inlet}^{1.42} * q^{0.283} * WTO^{0.95} * \left(\frac{L}{H}\right)^{0.71} \quad (2.34.)$$

The considered parameters in W_{Fuse} equation are geometrical shape and aerodynamic performance of UAVs based on design space constraints. As Zhang recommends K_{inlet} was assumed equal to one, which corresponds to an air intake pattern parameter K_{inlet} located at the fuselage nose [21, 24]. Since the baseline concept in this work is made of aluminum alloy, this correlation match well the current study. However, this will be further study for other types of materials used in the UAV industry.

2.2.1.4. Landing Gear Weight Estimation

The General Dynamic Method, described by Roskam [14], establishes a generalized correlation useful to calculate the Landing Gear Weight based on WTO. Equation 2.35 presents the landing gear weight estimation.

$$W_{LG} = 62.61 * \left(\frac{WTO}{1000}\right)^{0.84} \quad (2.35.)$$

2.2.2. Power Plant Weight Estimation

Aircraft Power Plant represents the energy source, transmission elements, and propulsion components mounted on the aircraft to propel it. The state of the art proposes several methods and considerations to calculate the Power Plant Weight. Nevertheless, for electric UAVs there is not a well-established method to define its weight contribution, this is mainly related to the numerous UAVs configurations, and hence, subsystems that are included. For this reason, based on similar propulsion configurations for UAS [9, 11, 15, 19] this work lays out a Power Plant estimating methodology combining these methods with well-known preliminary weight estimation methods used for civil aviation [14].

$$W_{PP} = W_{Motor} + W_{Gear} + W_{ESC} + W_{Batt} + W_{Prop} + W_{AI} + W_{PI} \quad (2.36.)$$

Equation 2.36 shows the subsystems involved in the power plant weight. For the sake of clarity, the description of the subsystems is divided into four sections. Firstly, the electric system is considered. Secondly, the battery weight calculation is described. Thirdly, the propeller weight estimation is shown, and finally, the air induction, and installation factors are described.

2.2.2.1. Electric System

The electric propulsion system comprises: electric motor, gearbox, and electronic speed controller. Equation 2.37 describes the parameters involved in its calculation. As observed, the electric motor maximum power P_{Max} is an important parameter to size the system, therefore, this has been defined based on Cinar's work [6], where a power-to-mass ratio of 5 [kW/kg] is given as reference value for this application.

$$W_{EPS} = W_{Motor} + W_{Gear} + W_{ESC} = \frac{P_{Max}}{5} + (0.0654 * P_{Max}) + (0.0362 * P_{Max}) \quad (2.37.)$$

2.2.2.2. Battery Weight Estimation

Battery weight depends on materials, number of cells, and battery characteristics. The correlation used in this work relates these parameters using the ratio between Battery

Maximum Power, and Battery Specific Power (BSP), as is shown in Equation 2.38 The advantage of this relation is that different battery types can be tested in the weight sensitivity analysis [25, 26].

$$W_{Batt} = \frac{P_{Max}}{BSP} \tag{2.38.}$$

2.2.2.3. Propeller Weight Estimation

Equation 2.39 is the correlation used for propeller weight estimation [14]. This correlation relates the number of blades per propeller, number of propellers, propeller diameter, number of engines, and the electrical motor maximum power [14, 25].

$$W_{Prop} = k_{Prop} * N_{Prop} * N_{Blades}^{0.391} * \left[\frac{D_P * P_{Max}}{N_E * 1000}\right]^{0.782} \tag{2.39.}$$

In Equation 2.39, k_{Prop}, refers to the type of engine mounted on the UAV. For this analysis the electric motor required corresponds to k_{Prop} equal to 15. This value corresponds to plastic, or composite engines below 50 [SHP]. In addition, it was assumed the number of propellers are equal to the number of engines. The propeller diameter, and maximum power are defined based on the case of study aircraft data.

2.2.2.4. Air Induction and Propulsion Installation Estimation

Roskam [14] proposes a correlation that involves the air induction and propulsion installation aspects. Equation 2.40 study the influence of aerodynamic, and technical aspects based on maximum power and number of engines [26].

$$W_{AI} + W_{PI} = 1.03 * (N_E)^{0.3} * \left(\frac{P_{Max}}{N_E}\right)^{0.7} \tag{2.40.}$$

2.2.3. Fixed Equipment Weight Estimation

Fixed Equipment (FE) has relation with the equipment carried onboard. Equation 2.41 is implemented for fixed equipment estimation. In this equation WFCS represents the

Flight Control System weight, WES is the Electrical System weight, WIAE considers the instrumentation, avionics and electronics equipment, and WPL is the Payload weight [27].

$$W_{FE} = W_{FCS} + W_{ES} + W_{IAE} + W_{PL} \tag{2.41.}$$

2.2.3.1. Flight Control System Weight Estimation

Equation 2.42 describes the flight control system weight, and considers system hardware such as: cables, pulleys, any required back-up structure, and push-rods. This correlation is applied for aircraft under 3629 [kg] of WTO equipped with mechanical flight controls [14].

$$W_{FCS} = 0.016 * WTO \tag{2.42.}$$

2.2.3.2. Electrical System Weight Estimation

The electrical system encompasses: power distribution units, converters, power system wiring harnesses, and in some cases, the generator [11]. For the present work, the correlation developed by Roskam [14] is utilized as shows Equation 2.43.

$$W_{ES} = 0.0268 * WTO \tag{2.43.}$$

2.2.3.3. Instrumentation, Avionics, and Electronic Systems

Equation 2.44 has been used to define the weight of instrumentation, avionics and electronic system [28]. Since the flight instruments weight is accounted in Equation 2.42, corresponding to the FE's subsection Flight Control System Weight Estimation, this has been neglected in the following expression [14].

$$W_{IAE} = \left[N_E * \left(5 + 0.006 * \frac{WTO}{1000}\right)\right]_{Engine} + \left[0.15 * \frac{WTO}{100} + 0.012 * WTO\right]_{Other} \tag{2.44.}$$

2.2.3.4. Payload Weight Estimation

Payload considers intelligence collection sensors such as: cameras, radars, EO/IR balls, among others [11]. Therefore, this weight contribution will depend directly on the UAV application. For the present study, different case scenarios for PA have been examined, using the aforementioned intelligence collection sensors.

3. RESULTS AND DISCUSSION

This section shows the obtained results from parametric codes to assess the weight and performance of an UAV in the Andean Region.

3.1. Model Validation

The validation process which has been divided in two represents the thesis core. Hence, in this current section is show the validation process, step by step, implemented in weight, and performance codes. At the beginning is detailed the database aircraft, and after that the numerical results obtained from the code application, in contrast to baseline numerical data.

3.1.1 Weight Model Validation

The flight height has been set as 3000 meters above sea level based on the Andean Region conditions. For the baseline aircraft data, the ITHACA 01 (**I**nformation, **T**echnology for **H**umanitarian **A**ssistance **C**ooperation and **A**ction), which is an electrical UAV of conventional configuration and is represented in a general way in Figure 3.1., has been selected [31, 32]. Table 3.1 shows the operating conditions for the case of study, and the main parameters of the baseline UAV.

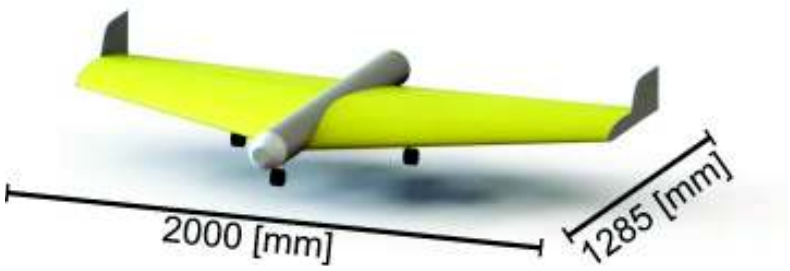

Figure 3.1. ITHACA CAD Model / Preliminary design [30].

Table 3.1. Operating conditions and main parameters.

Parameter	Value	Parameter	Value
Payload	0.25 [kg]	UAV Length	1.75 [m]
Mach Number	0.05	Region Altitude	3000 [m]
Wing Taper Ratio	0.65	Propeller Diameter	0.67 [m]
Wing Planform Area	2.1 [m2]	Battery Specific Power	1.5 [kW/kg]
Maximum Power	1.12 [kW]	Thickness to Chord Ratio	0.41

Table 3.2 shows the WTO, range and endurance results from ITHACA 01 and the study case. For a better understanding, the error between ITAHCA 01, and the Study Case has been estimated using Equation 3.1

$$Error\ \% = \frac{Teoric_{Value} - Experimental_{Value}}{Teoric_{Value}} * 100\% \tag{3.1}$$

Table 3.2. Model validation at cruise condition.

	WTO	Range	Endurance
ITHACA 01	13.98 [kg]	Limit: 15 [km] @ 15 [m/s]	30 [min] @ 15 [m/s]
Study Case	15.85 [kg]	Calculated: 11.62 [km] @ 9 [m/s]	24.6 [min] @ 9 [m/s]
Error	11.61%	22.50%	18%

As is observed in Table 3.2, the parametric method presents good accuracy compared with its simplicity, and low computing power demand. The largest error was presented for the Range calculation, that is attributed mainly to the parabolic drag model and the Oswald efficiency factor correlation, implemented by Samoylovitch [21]. In addition, the error in WTO affects Range and Endurance calculations, as both depend on this. Therefore, the errors presented in the previous mentioned performance parameters are larger than WTO. The simplicity of the parametric model does not consider materials, structural aspects, among others, which influenced on the WTO error.

3.1.2 Integrated Performance Model Validation

The integrated performance model will be validated based on kinematic parameters accuracy, and aerodynamic trends. Riboldi's work [19] will be use to validate the

kinematic parameters, and Ostler's research [31] to validate the aerodynamic characterization.

The Penguin BE is a lightweight electric-powered aircraft used by Riboldi. It is the selected baseline aircraft to evaluate the kinematic parameters at different mission stages [33, 34]. Figure 3.2. represents the Penguin B, and Table 3.3 shows the operating conditions presented by Riboldi, and the main parameters of the baseline UAV.

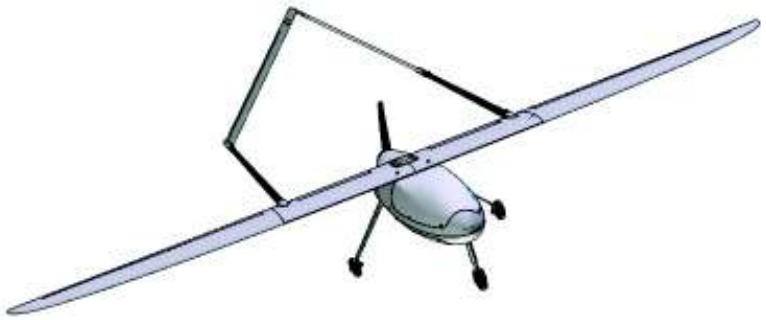

Figure 3.2. Baseline aircraft configuration [33].

Table 3.3. Baseline UAV operating conditions and main parameters.

Parameter	Value	Parameter	Value
WTO	21.5 [kg]	Aspect Ratio	30
Wing Span	3.3 [m]	Power Density	807.1 [Wh/kg]
Mach Number	0.146	Energy Density	145 [Wh/kg]
Wing Planform Area	0.79 [m2]	Battery Weight	4.41 [kg]
Maximum Battery Power	2700 [W]	Region Altitude	3000 [m]

Riboldi's research is the baseline to validate the integrated performance model in terms of kinematic parameters. It is focused on an integral approach to set up a stable and reliable sizing procedure for small lightweight aircraft [19]. The validation procedure establishes several geometric, power plant, and aerodynamic constraints to assess the UAV performance. Geometric, and Power Plant constraints involve aircraft specification, operation conditions, and electrical system features. The aerodynamic characterization is established by points at different mission stages considering:

zero lift-drag coefficient, maximum lift coefficient, and Oswald factor as is shown in Table 3.4.

Table 4.4. Polar coefficients [19].

Mission Stage	Clean	Takeoff	Landing
C_{D0}	0.011	0.031	0.101
C_{LMAX}	1.5	1.5	2.2
e	0.83	0.83	0.75

Based on the latter data, the proposed integrated performance methodology is validated by the comparison of kinematic parameters between the baseline aircraft information. Table 3.5 contrasts the proposed data from Riboldi, and the obtained data from the study case to carry out the model error using Equation 3.1.

Table 5.5. Validation of performance parameters.

Parameter	Baseline Results	Model Results	Error
ROC	2.02	2.55	26.24%
V_{Climb}	24.72	24.49	0.93%
V_{Cruise}	46.3	49.57	7.06%
$V_{Stalling}$	20.6	20.41	0.92%
Takeoff Ground Run	200	147.9	26.05%
Average Error			12.24%

As is observed in Table 3.5, the parametric method presents good accuracy compared with its simplicity, and low computing power demand. The largest error, with a value of 23.42%, is presented in the Rate of Climb estimation, and the takeoff run. This error is mainly attributed to the lack of information used for the aerodynamic characterization because the polar coefficients presented by Riboldi are general, but in the aircraft's design process the polar coefficients are variable, due to angle of attack, flight control surfaces, external factors, among others. On the other hand, the 2.81% of error presented in velocities calculation is negligible because of the method applied to calculate these parameters is commonly used in aircraft's preliminary design processes [10].

3.2. Cases of Study

The current section shows several studies applying weight, and integrated performance codes for UAVs in the Andean Region. It is focused on the identification of sensible variables in the aircraft design process.

3.2.1 Weight Analysis

The sensitivity analysis has been classified in three main components: structure, power plant, and fixed equipment as is indicated in Figure 3.3. A linear variation of each parameter has been examined against the main components weight and structural parameters can be defined based on geometric variables. Power plant has relation with energy sources, propulsion configuration, and energy management. For the case of fixed equipment the formulations presented by Roskam [14] give directly the linear correlations.

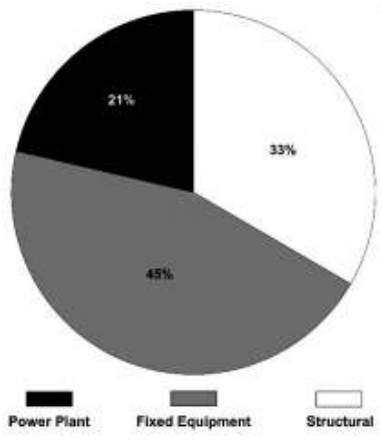

Figure 3.3. Weight distribution.

As is observed in figure 3.3., the largest weight share corresponds to fixed equipment, followed by structural and power plant components. This distribution is mainly related to several subsystems required for the autonomous flight and site-specific management used in UAVs. The largest contribution in this component belongs to the payload, hence this parameter has been selected as design space variable for the case scenarios in the following section. The structural contribution is mainly related to

fuselage and wings. In the case of fuselage, the model used corresponds to aluminum alloy, which is heavy compared to other UAV subsystems. In case of non-metallic light materials, which are widely used in UAV industry the structural contribution could decrease. This is an interesting aspect, which can be assessed in future work. Finally, the power plant weight share was mainly affected by the electrical motor maximum power, and the battery's specific energy. Since the previous parameters are defined by the type of battery, which has been explored in the case scenarios in the following section. To summarize, the component weight distribution highlights, which components should be resized in order to decrease WTO. In this work, three case scenarios were carried out to explore the WTO variation and its influence in UAV performance.

3.2.1.1. Weight Sensitivity Analysis

Weight module involves different parameters based on geometric, aerodynamic, and mechanic features. It is important to identify clearly the parameters of greatest influence. For this reason, a sensitivity analysis is a good statistical/analytical tool to implement into a parametric code that enables the identification of critical variables to optimize or reduce their influence.

The weight module is divided into three sub-modules: structural, power plant, and fixed equipment. Nevertheless, the sensitivity analysis considers structural, and power plant modules because the fixed equipment refers to optional onboard tools that enables the mission achievement. The following paragraphs describe the developed analysis used to identify sensible variables in the aircraft design space.

3.2.1.1.1. Structural

Figure 3.4. shows a sensitivity analysis developed for aircraft’s structure. It was taken from MATLAB’s weight module parametric code. The most important parameters in aircraft’s structural design are analyzed to evaluate their change influence into aircraft’s structural weight.

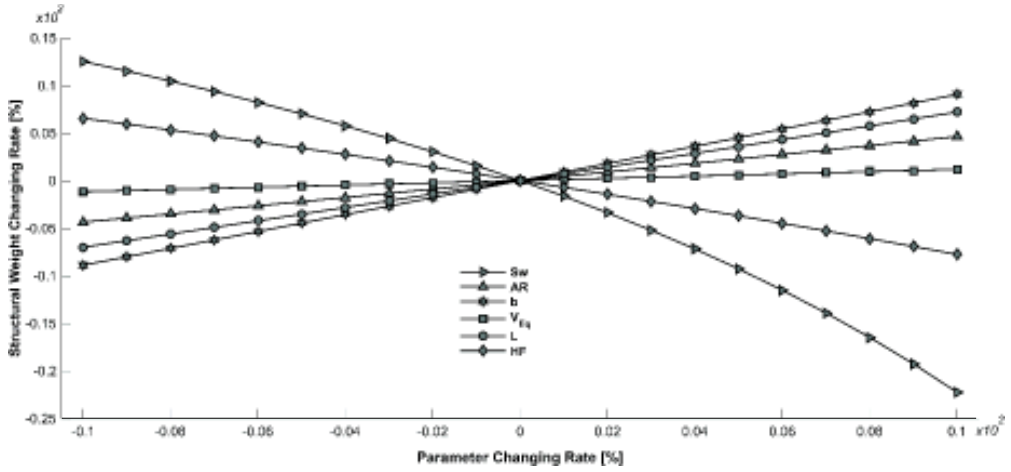

Figure 3.4. Structural sensitivity analysis.

The most important variables involved in the change of WTO are: aspect ratio, wing span, length, and fuselage height, which are geometric characteristics related with aircraft's weight and aerodynamic. In this context, equations represent the influence of parameter's change into WTO.

$$\Delta_{SW}\ [\%] = -0.754 * \Delta FH\ [\%] \tag{3.2}$$

According to Equation 3.2, the negative slope means a decrease of a unit in the Structural Weight (SW) is necessary to increase 0.754 times the fuselage height. For the remaining geometric features, the most influential parameters in the SW have been examined in the same way and their equations are as follows:

$$\Delta_{SW} = 0.51 * \Delta \mathrm{AR} \tag{3.3.}$$

$$\Delta_{SW} = 0.993 * \Delta \mathrm{b} \tag{3.4.}$$

$$\Delta_{SW} = 0.727 * \Delta \mathrm{L} \tag{3.5.}$$

The criteria selection considers the influence represented by slope value, though the sensitivity analysis was developed for most of the involved parameters.

3.2.1.1.2. Power Plant

Figure 3.5. is a sensitivity analysis developed for aircraft's power plant system in MATLAB.

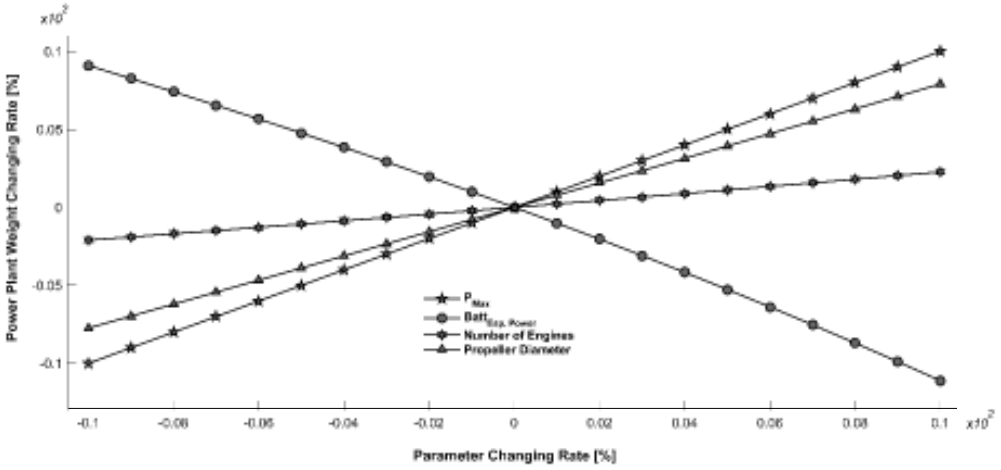

Figure 3.5. Power plant sensitivity analysis.

Propulsive architecture, energy source, and energy management are some of the criteria consider in the power plant estimation. Applying a sensitivity analysis was established that the most influence parameters are: maximum power, battery's specific energy, number of engines, and propeller's diameter as follows:

$$\Delta_{PPW} = \Delta \mathrm{P}_{Max} \tag{3.6.}$$

Equation 3.6 shows a positive direct relation between Maximum Power and Power Plant Weight (PPW). Hence, Δ_{PPW} increases in the same magnitude of $\Delta_{P_{Max}}$. The following equations, from 3.7 to 3.9, have been examined in a similar way.

$$\Delta_{PPW} = -1.072 * \Delta \mathrm{E}_{Esp} \tag{3.7.}$$

$$\Delta_{PPW} = 0.231 * \Delta \mathrm{E}_{Number} \tag{3.8.}$$

$$\Delta_{PPW} = 0.810 * \Delta \phi_{Prop} \tag{3.9.}$$

For the aforementioned equations is deduced that Δ_{PPW} highly depends on ΔE_{Esp} due to the negative slope, and in a minor percentage of ΔE_{Number}. From these results is highlighted the importance of geometric and propulsive parameters in UAV preliminary design because of the parameters influence in different areas such as: weight, aerodynamic, size, shape, propulsive architecture, among others.

3.2.2. Performance Analysis at Cruise Condition

In the following sections is described the influence of WTO in UAV performance. For this purpose, three case scenarios have been defined based on main design space variables, which were defined from the previous weight sensitivity analysis. The design space variables examined are: number of engines, battery's type, and payload.

Based on Bendea's [30] publication, ITHACA 01 is a UAV with a Range less than 10 [km], endurance of approximately of 1 [hour], and a total mass of 5 [kg]. Table 3.6 shows the three cases scenarios. The number of engines, battery's type, and payload configuration vary in cases one, two, and three, respectively.

Table 6.6. Case scenarios.

	Number of Engines	Battery's Type	Payload Configuration
Case 1	From 1 to 6	Li-Ion	Adapted Camera
Case 2	1	LiPo / Zn-Air / Li-Ion	Adapted Camera
Case 3	1	Li-Ion	TIU / MSC / EO/IR / AC

As is observed in figure 3.6., an increment in the number of engines reduces Endurance and Range. This trend is mainly related to the engine's weight model implemented in the present work and the assumptions made to size the propulsion system based on the electrical motor maximum power. For this study, it is assumed that the maximum power will be linearly reduced by the increment in number of engines, at this stage of the study this assumption is good enough, however this should be refined by using a propulsion model. According to the trends observed in the previous figure, can be concluded that for Endurance and Range is better to have one large engine rather than several small ones. The previous is concluded without

considering other aircraft performance aspects such as: aerodynamics, structural design, reliability, among others.

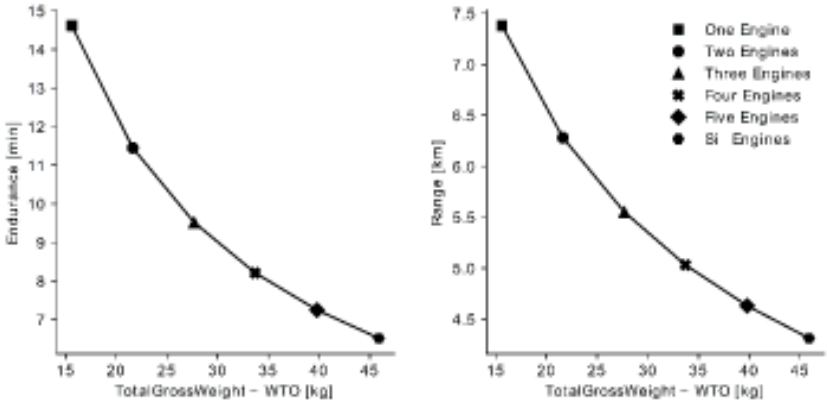

Figure 3.6. Performance parameters based on the number of engines.

Figure 3.7. shows the influence of battery's type in WTO, Endurance, and Range. For this case, were selected three types of batteries: LiPO batteries, Li-Ion batteries, and Zn-Air batteries. From the figure can be concluded that Li-Ion battery is the best case, since they present higher specific energy and therefore contribute less to WTO.

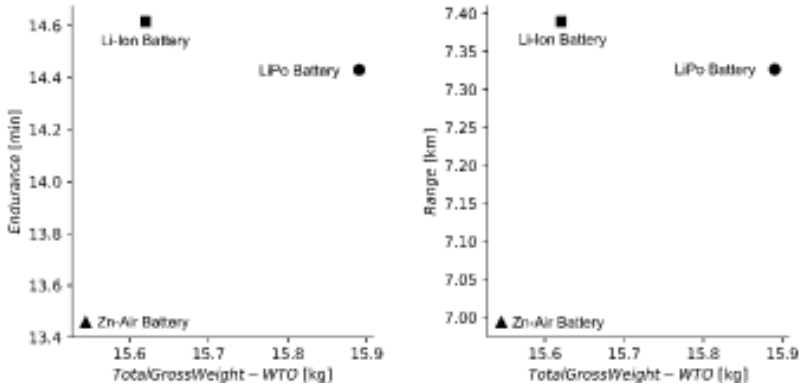

Figure 3.7. Performance parameters based on battery's type.

The last case of study makes an identification of payloads influence in endurance and performance. Based on site specific management applications were consider four cameras. Starting with an adapted camera that use filters to choose correct band in the light spectrum, an EO/IR camera, a multi-spectral, and a thermal camera. The aforementioned cameras are implemented in PA, but each one has different characteristics regarding their capabilities for data collecting.

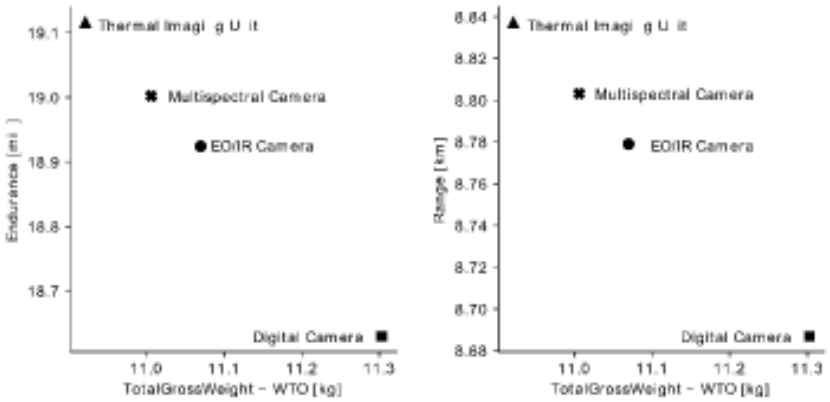

Figure 3.8. Performance parameters based on camera selection.

Figure 3.8. shows the influence of cameras' weight in endurance and range. As observed, camera selection has significant influence in UAV endurance, but its effect is not as large for the case of range. Nowadays, thermal cameras have been enhanced in terms of size, performance, energy consumption, and utility, and hence their weight contribution is the lowest in the present analysis. The application of multi-spectral and thermal cameras translates to accurate imaging collection with an optimal energy consumption, however their cost is a main drawback.

3.2.3 Integrated Performance: Aerodynamic Characterization

Ostler's research is used to validate the accuracy of aerodynamic parameters calculated in the integrated performance module. Ostler's work is based on a performance flight testing of small, electric-powered UAVs [31]. An advantage of this work is the facility to obtain the aircraft's aerodynamic characterization represented by a second order polynomial equation in the lift-drag parabolic form [7, 10, 33]. On the other hand, it is important to consider that this work has a lack of aircraft specifications, energy system, and energy sources data. Hence, the validation of aerodynamic models will be done considering the latter validation process, and the plots presented in Ostler's work.

Figure 3.9. is the drag polar curve analytically-estimated by the aerodynamic characterization module integrated in the performance study. In addition, this drag polar curve is superimposed on flight test results represented in Ostler's research [31]. The latter research applies the lift-drag parabolic approximation to study the aerodynamic characterization. Hence, Equation 3.10. represents the aircraft aerodynamic performance at an unknown flight point.

$$C_D = C_{D0} + K \times C_L^2 = 0.015 + 0.13 \times C_L^2 \quad (3.10.)$$

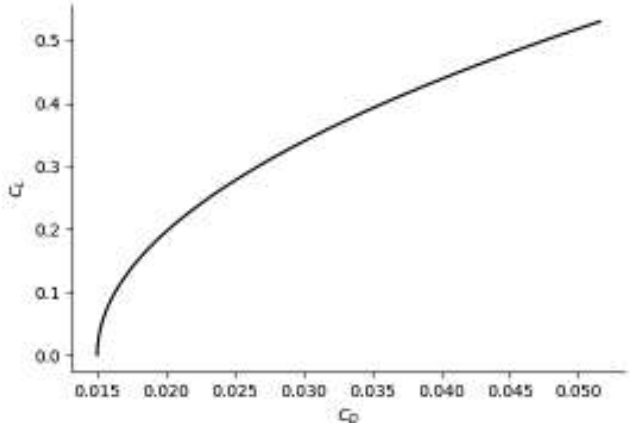

Figure 3.9. Integrated Performance Drag Polar Estimation.

Furthermore, figure 3.10. shows the performance diagram obtained from the integrated performance study. This diagram is also known as Penaud Diagram. It is useful to demonstrate the airspeed requirements, limitans (V_s, V_{Max}), and optimal points to flight (V_{MPR} = $V_{Minimum\ Power\ Required}$).

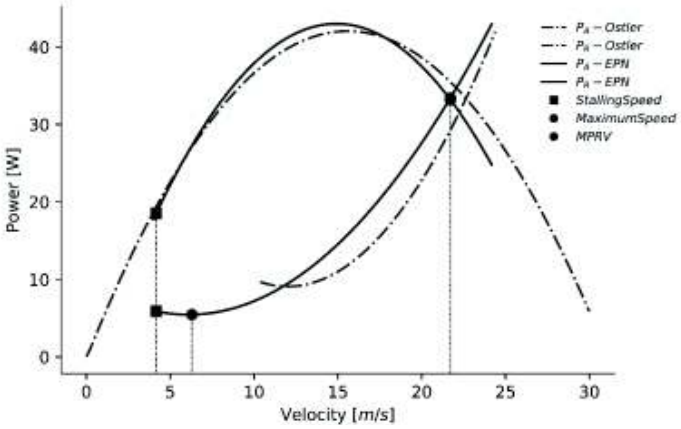

Figure 3.10. Integrated Performance Power Diagram.

Penaud diagram is based on aircraft's aerodynamic characterization. Hence, at each mission segment it changes due to angle of attack, air flow conditions, and power distribution. In this way, Ostler's work was superimposed in results obtained from the EPN model, in order to demonstrate the trend between experimental and analytical curves [31]. To achieve this goal, it was necessary to make a fitting process in the Power Available curve because Ostler's paper does not have enough information about energy system, and energy resources system. Nevertheless, the Power Required curve maintain a constant trend when is assumed that 6 [W] are drawn from the energy source to supply the avionics, and payload power requirement in an unknown mission segment.

3.2.4. Integrated Performance: Kinematic & Energy Analysis

Being sure about the error in the kinematic parameters, and the trend in the aerodynamic characterization. The integrated performance study will continue defining the aircraft design space for the Penguin B because the operating conditions, and specifications of this aircraft are known.

In this way, the integrated performance analysis considers the analysis of takeoff, and landing maneuvers. The takeoff maneuver is composed of three different stages. The first one is the ground run at which the most important parameter is ground run distance. The second is the airborne phase which is defined by the airborne path radius, and flight-path angle. Finally, the climb is the last stage, well-defined by the rate of climb. The kinematic parameter that defines the takeoff maneuver is the stalling speed because it is the pivot to determine the rotation speed, liftoff velocity, unstick velocity, and climbout velocity as was explained in Takeoff Maneuver Section [10]. The landing maneuver is composed of three phases: airborne distance, touchdown, and landing ground run. The most important parameters to calculate in latter stages are: airborne radius of curvature, flight-path angle, and standstill distance or horizontal distance.

Table 3.7 shows the physic preliminary design parameters estimated by the integrated performance code to study the takeoff, and landing maneuvers. In this case, it is not

possible to establish a comparison between the baseline, and the study case aircraft because Riboldi's research does not present the result of these parameters. Nevertheless, the performance physic parameters are based on kinematic performance parameters, hence the error for these parameters is 12.3% too.

Table 3.7. Integrated performance physic parameters.

Parameter	Takeoff	Landing
Flight Path Angle [deg]	1.27	4.03
Horizontal Distance [m]	124.19	856.58
Radius of Curvature [m]	18.74	212.5

Figure 3.11. represents the integrated mission power distribution. There is remarkable that over the 2700 [W] storage in batteries, the entire mission uses 621 [W] (23%), considering that the takeoff maneuver drew the 135 [W] (5%), and the energy consumption in cruise condition represents 486 [W] (18%). These results demonstrate an irregular power distribution with non-use power. It is because Riboldi's research is focused on preliminary weight sizing instead of performance parameters, and power consumption.

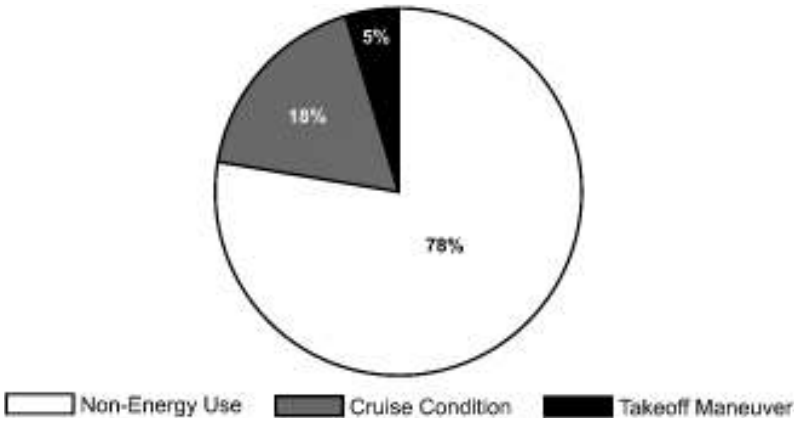

Figure 3.11. UAV power distribution.

The latter figure encourages optimization possibilities in terms of energy for the study case. The remaining power can be drawn by high fidelity avionics instrumentation or different cameras such as: thermal units, EO/IR, multispectral, among others. Another way to use the remaining power is stablishing new flight conditions to improve the aircraft's range, and endurance. In this way, there are multiple possibilities to improve the UAV performance, hence the following sub-sections establish many sensitivity

analyses to recognize the weight, and geometric influence into energy distribution, and physical aspects.

3.2.5. Integrated Performance: Sensitivity Analysis

The integrated performance analysis involves different aspects from the aircraft space design. In the following sub-sections, the most relevant parameters are described to understand their influence in flight performance.

3.2.5.1. Ground Run Distance due to Payload, and Friction Coefficient.

This section shows the Penguin B [32] performance parameters variation when payload varies. The considered payloads for this study were the following cameras: digital camera (Sony WX500 [34]), multispectral camera (RedEdge MicaSense [34]), EO/IR camera (M2-D Stabilized OE IR-FLIR [34]), and a thermal unit (M1-D UAV Gimbal [34]).

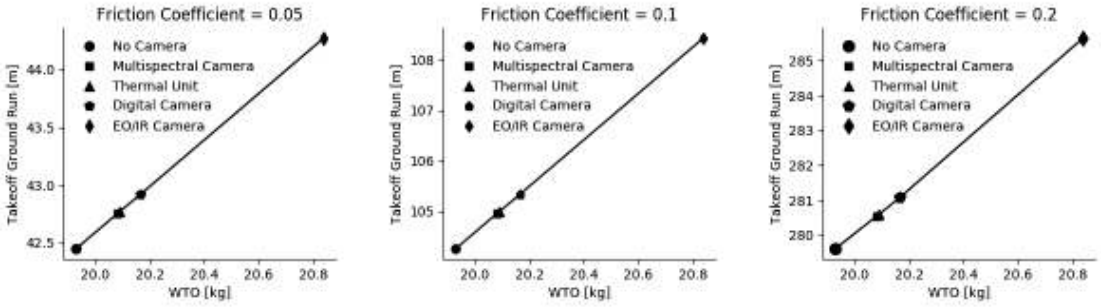

Figure 3.12. Takeoff ground distance due to payload, and friction coefficient.

Figure 3.12. represents the variation of takeoff ground distance at different friction coefficients, when no-cameras, and different cameras are incorporated in the UAV weight. The latter figures highlight that the impact of fixed equipment weight variation can be neglected, but the friction coefficient variation produces a completely different takeoff ground distance that significantly affect the aircraft preliminary design. In this way, the ground run distance varies in more than 600% between an UAV assembled with a digital camera that makes the takeoff maneuver in a ground with a friction

coefficient equal to 0.05, and the same aircraft that makes the takeoff maneuver in a ground with a friction coefficient equal to 0.2. The positive slope obtained from the variation between payload's weight, and takeoff ground run distance is based on the highly influence of weight. However, the most representative aspect to consider is the friction coefficient which is involved in the distance calculation.

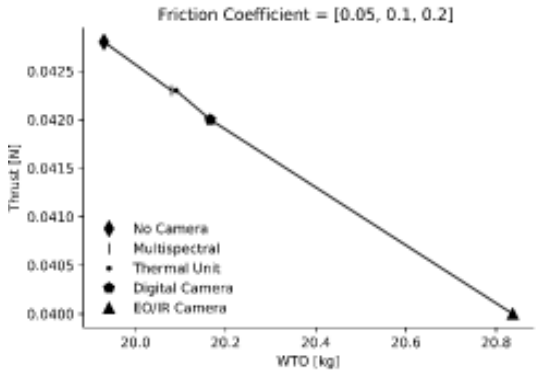

Figure 3.13. Thrust due to payload, and friction coefficient.

Similarly, figure 3.13. shows the thrust variation at different friction coefficients, when no-cameras, and different cameras are incorporated in the UAV. This figure demonstrate that the thrust force required for takeoff ground run does not depend on ground friction coefficient. Nevertheless, weight variation affects thrust requirements. In contrast with figure 3.12., aircraft kinematic performance aspects (Thrust) are not related with physic parameters (Ground Run Distance). The negative slope demonstrates the lower influence of weight components into propulsion system. It is because the propulsion is direct related with aerodynamic, and kinematic features.

3.2.5.2. Range, and Endurance due to Maximum Power, and Altitude.

To study the influence of maximum power, and altitude into range and endurance was taken from the open domain the most typical batteries used in UAVs. The state of the art shows that batteries of 1300 [W], 1940 [W], 2700 [W], 3530 [W], 4000 [W], and 4200 [W] are commonly used as UAVs power plant units [19]. Based on batteries' weight, and considering the sensitivity analysis proposed in equation 3.6 was stablished the WTO variation, and the effect caused in range, and endurance.

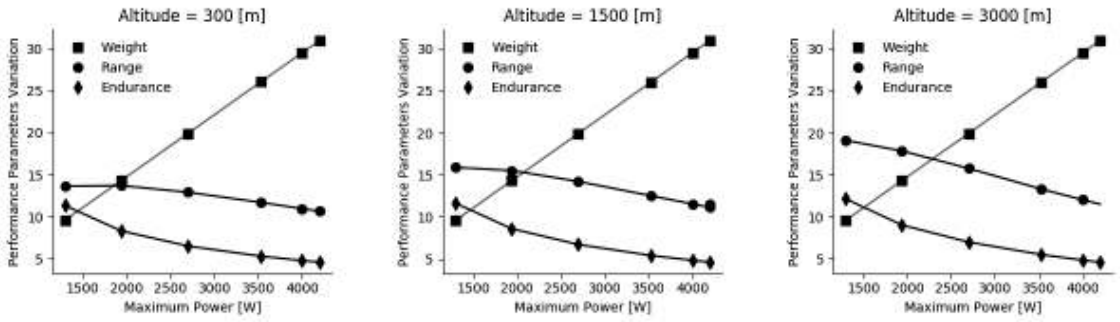

Figure 3.14. Range, and endurance due to maximum power, and altitude.

Figure 3.14 ratify the power plant sensitivity analysis showing a positive slope curve that represents the linear variation between weight, and maximum power. A remarkable aspect in this figure is that range and endurance decrease when maximum power increases, but range and endurance rise at higher altitudes. The highest, and lowest variation in range is presented when a power plant of 1300 [W], and 4200 [W] are installed, respectively. The range obtained at sea level (300 *[m]*) in contrast to the range obtained at highland (3000 *[m]*) varies in 40%, and 8% when batteries of 1300 [W], and 4200 [W] are assessed. Similarly, the highest, and lowest variation in endurance is presented when a power plant of 1300 [W], and 4200 [W] are installed. The endurance obtained at sea level (300 *[m]*) in contrast to the range obtained at highland (3000 *[m]*) varies in 7%, and 0.4% when batteries of 1300 [W], and 4200 [W] are assessed. Based on the latter data, it is important to remark that high-altitude regions in combination with low power batteries (WTO reduction) improve range, and endurance in UAVs. For the aforementioned results, it is clear that performance parameters depend on power plant capacity, and weight variation induced by batteries. It is important to recall that aircraft performance is improved at high altitude regions for air density influence.

3.2.5.2. Range, and Endurance due to Aspect Ratio, and Altitude.

To study the influence of aspect ratio, and altitude in range, and endurance was taken five different UAVs from Riboldi's research [19]. The baseline UAVs selected from Riboldi's research [19] were: Silent 2 (AR=13.7), Taurus Electro G2 (AR=18.6), Penguin B (AR=22.46), ElectroLight 2 (AR=30), and Antares 20E (AR=31.7).

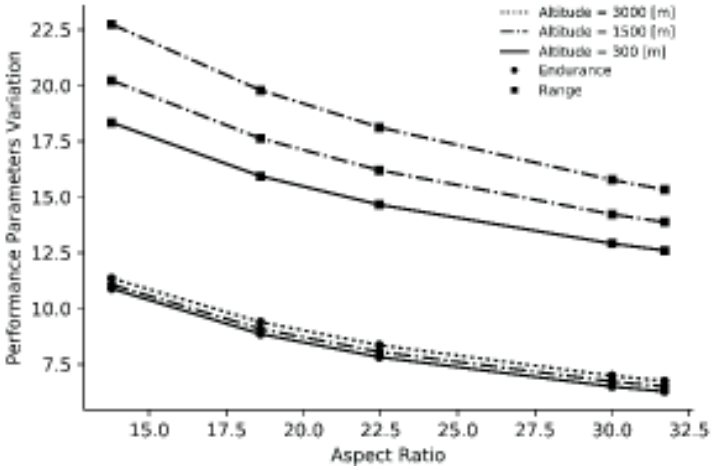

Figure 3.15. Range, and endurance due to aspect ratio, and altitude.

Figure 3.15 shows a negative slope between aspect ratio, and performance parameters. The average variation of range, and endurance for different aspect ratio, and altitude are 18.78%, and 6%, respectively. In addition, the latter figure shows that high altitude regions, and low aspect ratio values improves performance parameters. Based on the latter figure, aspect ratio has direct influence in aircraft geometry, power requirements, and aerodynamic characterization.

4. CONCLUSIONS

This work highlights the relation between weight and performance, considering geometrical and energy source characteristics of electric-powered UAVs ranging from SUAS to HALE UAVs. The developed method enables a versatile and low computing demanding modelling compared to high fidelity tools. The general assessment methodology divided the weight, and integrated performance module in different sub-systems to assess the weight and performance of unmanned aerial vehicles in the Andean Region.

Aircraft preliminary space of design is defined by weight module. It is composed of three components, which are: structural, power plant, and fixed equipment. The weight structural component is highly influenced by the wing span and the fuselage height. The power plant component is composed of: electrical system, battery, propeller, and air induction/installation weights. From the analysis of the aforementioned parameters, it was identified that the power plant weight is highly affected by battery's specific energy and electric maximum power. The validation process reflects an average error of 11.61% for this module.

Integrated performance can be highly improved by the reduction of WTO. In the best-case scenario at cruise condition, it was found that a reduction of 1.8% of WTO translates to an increment in range of 1.09%, and endurance of 1.03%. In addition, the results obtained from integrated performance reflects an average error of 12.3% for performance parameters. The sensitivity analysis demonstrate that high altitude regions improve aircraft performance, and the friction coefficient greatly affects the physic parameters.

To summarize, the proposed parametric model for weight and performance assessment is a multipurpose tool for preliminary UAV design that can be enhanced with the implementation a refined parametric aerodynamic, and power plant model.

REFERENCES

[1] F. G. Harmon, A. A. Frank, and J. Chattot, “Conceptual Design and Simulation of a Small Hybrid-Electric Unmanned Aerial Vehicle,” *J. Aircr.*, vol. 43, no. 5, pp. 1490–1498, 2006.

[2] L. W. Traub, “Erratum: Unified Approximation for Nonparabolic Drag Polars,” *J. Aircr.*, vol. 44, no. 2, pp. 702–702, 2007.

[3] A. A. De Paula, M. S. De Sousa, and I. Researcher, “Drag polar prediction methodologies during aircraft design phases,” no. January, pp. 1–19, 2017.

[4] S. G. Kontogiannis and J. A. Ekaterinaris, “Design, performance evaluation and optimization of a UAV,” *Aerosp. Sci. Technol.*, vol. 29, no. 1, pp. 339–350, 2013.

[5] G. Avanzini, E. L. De Angelis, and F. Giulietti, “Optimal performance and sizing of a battery-powered aircraft,” *Aerosp. Sci. Technol.*, vol. 59, no. October, pp. 132–144, 2016.

[6] G. Cinar, M. Emeneth, and D. N. Mavris, “A Methodology for Sizing and Analysis of Electric Propulsion Subsystems for Unmanned Aerial Vehicles,” *54th AIAA Aerosp. Sci. Meet.*, no. January, pp. 1–11, 2016.

[7] E. Torenbeek, *Synthesis of Subsonic Airplane Design: An Introduction to the Preliminary Design of Subsonic General Aviation and Transport Aircraft With Emphasis on Layout, Aerodynamic Design, Propulsion, and Performance*, First Ed. Delf, The Netherlands: Delf Univ. Pres, 1982.

[8] K. M. Tsang, W. L. Chan, and Y. K. Wong, “Lithium-ion Battery Models for Computer Simulation *,” no. 2, pp. 98–102, 2010.

[9] W. A. Mair and D. L. Birdsall, “Aircraft performance,” no. February, p. 300, 1998.

[10] G. Ruijgrock, *Elements of Aircraft Performance*, Second Ed. Leeghwasterstraat, The Netherlands: VSSD, 2009.

[11] J. Gundlach, “Designing Unmanned Aircraft Systems: A Comprehensive Approach,” *Aurora Flight Sci.*, p. 869, 2011.

[12] M. C.-Y. Niu, “Airframe Structural Design: Practical Design Information and Data on Aircraft Structures,” *GTRI Project A-5636 Technical Report Final Report ….* 1988.

[13] E. Valencia, V. Hidalgo, and O. Calle, “Weight and Performance Methodology of an UAV at Cruise Condition for Precision Agriculture,” *AIAA Pap.*, no. August,

pp. 1–15, 2017.

[14] J. Roskam, C. Tau, and E. Lan, “Airplane Aerodynamics and Performance.” p. 110, 1997.

[15] Z. Yi and W. Heping, “A study of structure weight estimating for High Altitude Long Endurence (HALE) Unmanned Aerial Vehicle (UAV),” *ICAS-Secretariat - 25th Congr. Int. Counc. Aeronaut. Sci. 2006*, vol. 3, pp. 1784–1789, 2006.

[16] C. Pornet *et al.*, “Methodology for Sizing and Performance Assessment of Hybrid Energy Aircraft,” *J. Aircr.*, vol. 52, no. 1, pp. 1–12, 2014.

[17] M. Saarlas, “Aircraft Performance,” *Aircr. Perform.*, pp. 1–282, 2007.

[18] A. Altman, “A Parametric Study On Design Variables Effecting Hale UAV Aircraft Design For A Conventional Configuration,” *1st UAV Conf.*, no. May, pp. 1–12, 2002.

[19] C. E. D. Riboldi and F. Gualdoni, “An integrated approach to the preliminary weight sizing of small electric aircraft,” *Aerosp. Sci. Technol.*, vol. 58, no. July, pp. 134–149, 2016.

[20] A. Abbas, J. De Vicente, and E. Valero, “Aerodynamic technologies to improve aircraft performance,” *Aerosp. Sci. Technol.*, vol. 28, no. 1, pp. 100–132, 2013.

[21] O. Samoylovitch and D. Strelets, “Determination of the Oswald efficiency factor at the aeroplane design preliminary stage,” *Aircr. Des.*, vol. 3, no. 3, pp. 167–174, 2000.

[22] A. Altman, “A comparative study to identify the propeller-driven hale UAV configuration with the maximum endurance performance,” *1st UAV Conf.*, no. May, pp. 1–11, 2002.

[23] K. Chang, P. Rammos, S. A. Wilkerson, M. Bundy, and S. A. Gadsden, “LiPo battery energy studies for improved flight performance of unmanned aerial systems,” vol. 9837, p. 98370W, 2016.

[24] B. Saha *et al.*, “Battery Health Management System for Electric UAVs,” pp. 1–9, 2011.

[25] O. Gur and A. Rosen, “Optimizing Electric Propulsion Systems for Unmanned Aerial Vehicles,” *J. Aircr.*, vol. 46, no. 4, pp. 1340–1353, 2009.

[26] A. Sobester and A. J. Keane, “Multidisciplinary design optimization of UAV airframes,” *Adv. Eng. Softw.*, vol. 36, no. 5, pp. 301–311, 2006.

[27] R. Austin, *Unmanned Aircraft Systems*. 2010.

[28] C. Grano-Romero, M. Garcia-Juarez, J. F. Guerrero-Castellanos, W. F. Guerrero-Sanchez, R. C. Ambrosio-Lazaro, and G. Mino-Aguilar, “Modeling and control of a fixed-wing UAV powered by solar energy: An electric array reconfiguration approach,” *Int. Power Electron. Congr. - CIEP*, vol. 2016–Augus, pp. 52–57, 2016.

[29] H. Bendea, F. Chiabrando, F. G. Tonolo, and D. Marenchino, “MAPPING OF ARCHAEOLOGICAL AREAS USING A LOW-COST UAV THE A UGUSTA BAGIENNORUM TEST SITE,” no. October, pp. 1–6, 2007.

[30] H. Bendea *et al.*, “LOW COST UAV FOR POST-DISASTER ASSESSMENT,” pp. 1373–1380.

[31] J. N. Ostler, W. J. Bowman, D. O. Snyder, and T. W. McLain, “Performance Flight Testing of Small, Electric Powered Unmanned Aerial Vehicles,” *Int. J. Micro Air Veh.*, vol. 1, no. 3, pp. 155–171, 2009.

[32] U. Factory, “Penguin B Datasheet.” UAV Factory USA LLC, Irvington, NY, p. 8, 2015.

[33] U. Factory, “Penguin B Interactive 3D.” UAV Factory USA LLC, Irvington, NY, p. 1, 2015.

[34] J. Taylor, “Event 38 – Unmanned Systems,” *E384 Complete Package*, 2017. [Online]. Available: https://event38.com/product/e384-complete-package-4/. [Accessed: 01-Oct-2017].

APPENDIX

A1. Typical Variation of Thrust with Mach Number

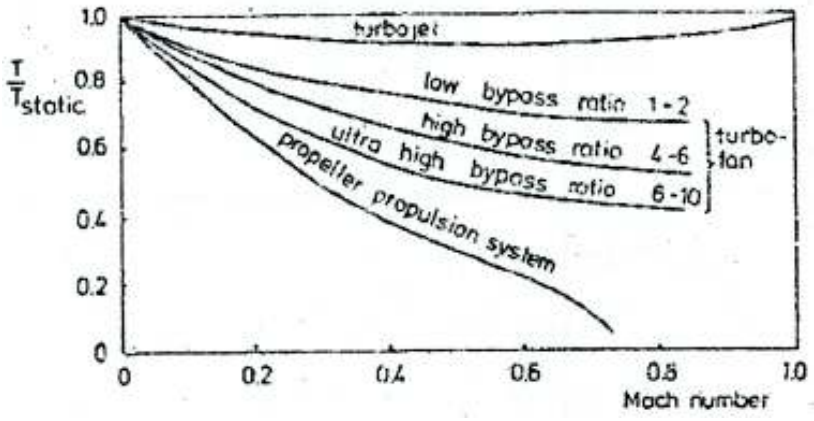

Elements of Airplane Performance, Ruijgrock, G., Chapter 9, Figure 9.11 [10].

A2. Propellers Chart of 2-Bladed Propeller (Estimated)

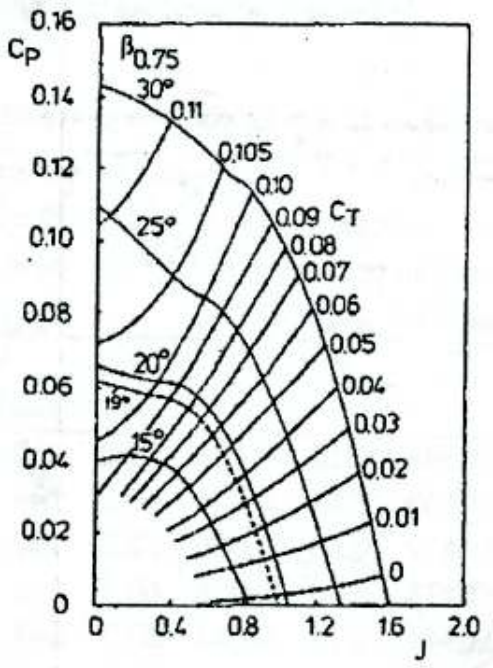

Elements of Airplane Performance, Ruijgrock, G., Chapter 9, Figure 9.14 [10].

A3. MATLAB Code for Weight Estimation

```
clc, clear, close all

WToH=10E7;                  % Maximum WTO [lbs]
WToL=0;                     % Minimum WTO [lbs]
WToG=(WToH+WToL)/2          % Mean WTO[lbs]
k=1;                        % Counter

while (k==1)

%%%%% AIR PROPERTIES / ISA

H=2850;                     % Flight Height
M_cr=0.059;                 % Flight Mach Number
RGases=287.05;              % Constant of Gases
r=1.4;                      % Adiabatic Index of Air
ro_sl=0.07441;              % [lb/ft3]

if H < 11000
    t_amb = 288.15-0.0065*H;
% Surrondings Temperature [k]
    p_amb = 101325*(1-0.0000226*H)^(5.256);
% Static Pressure [Pa]
    ro_amb = 1.226*(1-0.0000226*H)^(5.256);
% Density [kg/m^3]
    a_amb = (r*RGases*t_amb)^0.5;
% Speed of Sound [m/s]

else

    t_amb = 271.15-56.5;
% Surroundings Temperature [k]
```

```
    p_amb = 22557.74*exp(-(H-11000)/6341.33);
% Static Pressure [Pa]
    ro_amb = 0.363*exp(-(H-11000)/6341.33);
% Density [kg/m^3]
    a_amb = (r*RGases*t_amb)^0.5;
% Speed of Sound [m/s]
End

   V0= M_cr*a_amb;
% Aircraft Speed [m/s]
   Tamb = t_amb * (1+M_cr^2*(r-1)/2);
% Surroundings Temperature
   Pamb = p_amb * (1+M_cr^2*(r-1)/2)^(r/(r-1));
% Surroundigs Pressure
   ro_ambi=ro_amb*0.062482
% Density [lb/ft3]
   V01 = M_cr*a_amb;
% Speed @ Mach Number [m/s]
   V0=V01*3.28084;
% Speed @ Mach Number [ft/s]
   Tamb = t_amb * (1+M_cr^2*(r-1)/2);
% Surroundings Temperature
   Pamb = p_amb * (1+M_cr^2*(r-1)/2)^(r/(r-1));

%%%%% STRUCTURE WEIGHT

%%%% - WING WEIGHT / ROSKAM (5.2) & CHUN (16.2.2)

Ct=2.7493;          % Tip Chord [ft]
Cr=4.2192;          % Root Chord [ft]
lambda=(Ct/Cr);     % Taper Ratio
Nz=1;               % Ultimate Load Factor [g]
b=6.5617;           % Wing Span [ft]
```

```
Sw=22.6042;          % Wing Planform Area [ft2]
AR=(b^2)/Sw ;        % Wing Aspect Ratio
u=(0.4183/3.4843);   % u=(t/c) Max. Thickness/ Chord Length
da=0;                % Wing 1/2 Chord Sweep Back Angle [°]
Ve=V0*((ro_ambi/ro_sl)^0.5); % Speed [ft/s]
Vei=Ve*1.68781;      % Equivalent Velocity [KNOTS]
% Material Stress | Ultimate Load Factor
n=(log((0.1*WToG)/(0.04674*(WToG^0.397)*(AR^1.712)))/(log(Sw)*
0.143))

WWing=96.948*((((WToG*n/10E5)^0.65)*((AR/cos(da))^0.57)*((Sw/1
00)^0.61)*(((1+lambda)/(2*u))^0.36)*((1+(Vei/500))^0.5))^0.993
) % [lb]

%%% - EMPENNAGE / GUNDLACH (6.39)

WAEmp=0.5;       % Aerial Weight of the Tails
SEmp=2.34;       % Empennage Planform Area [ft2]

WEmp=WAEmp*SEmp                              % [lb]

%%% - FUSELAGE / ICAS 2006

q=0.5*ro_ambi*(V0^2);    % Dynamic Pressure [ft/s2]
Ki=1;                    % Air intake Pattern parameter
[1/1.05/1.2]
L=5.7415;                % Fuselage Length [ft]
HF=0.6616;               % Fuselage Structure Height [ft]

WFusea=0.0025*(Ki^1.42)*(q^0.283)*((WToG)^0.95)*((L/HF)^0.71)
WFuse=WFusea*2.2                             % [lb]

%%%% - LANDING GEAR / ROSKAM GD METHOD
```

```
WLG=62.61*((WToG/1000)^0.84)                % [lb]

%%%% - TOTAL WEIGHT - %%%%

WStructure=WWing+WEmp+WFuse+WLG             % [lbs]

%%%%% POWER PLANT WEIGHT

%%%% - ELECTRIC PROPULSION SYSTEM = Motor + Gear + ESC /
GUNDLACH (6.50)

PMax=1.5;        % [kW]
WMotor=PMax/5    % Gokcin - Electric Motors

WEPSa=WMotor+(0.054*PMax)+(0.0362*PMax) % [kg]
WEPS=WEPSa*2.2 % [lb]

%%%% - BATTERY WEIGHT

bed=1.4914;          % Battery Specific Power [kW/kg]

WBa=PMax/bed         % [kg]
WB=WBa*2.2           % [lb]

%%%% - PROPELLER WEIGHT / ROSKAM GD METHOD (6.13)

kProp=15;        % Multiplication Factor
NEng=1;          % NProps = NEngines IV
NBlades=2;       % Number of Blades
D=2.24;          % Propeller Diameter [ft]
PMaxi=PMax*1.34102;      % Maximum Power [kW]
```

```
WProps=(kProp*NEng*(NBlades^0.391)*(((D*PMaxi)/(1000*NEng))^0.
782)) % [lb]

%%%% - AIR INDUCTION + INSTALLATION / ROSKAN | TORENBEEK (6.8)

Wai=(1.03*((NEng)^0.3)*((PMaxi/NEng)^0.7));      % [lb]

%%%% - TOTAL WEIGHT - %%%%

WPowerPlant=WEPS+WB+WProps+Wai                    % [lb]

%%%%% FIXED EQUIPMENT

%%%% - FLIGHT CONTROL SYSTEM / ROSKAN CESSNA METHOD (7.1)

Wfc=0.016*WToG;      % [lb]

%%%% - ELECTRICAL SYSTEM / ROSKAN CESSNA METHOD (7.12)

Wes=0.0268*WToG;     % [lb]

%%%% - INST + AVIONICS + ELECTRONICS / ROSKAM GD (7.23)

Wi=(NEng*(5+0.006*(WToG/1000)))+(0.15*(WToG/1000)+(0.012*WToG)
);   % [lb]

%%%% - PAYLOAD / DATA SHEET

WPL=4; % [lb]

%%%% - TOTAL WEIGHT - %%%%

WFixedEquipment=Wfc+Wes+Wi+WPL % [lb]
```

```
%%%%% TOTAL RESULT

WTotal=WFixedEquipment+WPowerPlant+WStructure

%%%%%%%%%%%%%%%%%%%%%%%%%%%%%%%%%%%%%%%%%%%%%%%

WToCal=(WPL+(Wi+Wes))/(1-
(1/WToG)*(WStructure+WPowerPlant+WFixedEquipment))

DiffWTo=abs((WToG-WToCal)/WToG)
    if (DiffWTo<0.003)
                WToDesign=WToG
                k=0;
            else
            if (WToG<WToCal)
                WToL=WToG;
                WToG=(WToH+WToL)/2;
            else
                WToH=WToG;
                WToG=(WToH+WToL)/2;
            end
            k=1;
    end
end

title('ITHACA GLOBAL WEIGHT EVALUATION')
G=[WPowerPlant WFixedEquipment WStructure];
pie(G)
legend('Propulsion','Fixed Equipment','Structural')
```

A4. MATLAB Code for Integrated Performance Assessment

```
clear all, clc, close all

% Inputs [SI]

% Aircraft Specifications

W=21.5;              % Weight [kg]
Sw=0.79;             % Wing Planform Area [m2]
b=3.3;               % Wing Span [.]
A=30;                % Aspect Ratio [DL]
Ct=0.0785;           % Tip Chord [m]
Cr=0.314;            % Root Chord [m]
lbd=(Ct/Cr);         % Taper Ratio [.]
HF=0.193;            % Fuselage Height [m]
fw=0.288;            % Fuselage Width [m]

% Operating Data

H=10;                 % Initial Altitude [m]
Hth=160;              % Theorical Altitute [m]
CD0=0.048;            % Zero Lift-Drag Coefficient
g=9.8;                % Gravity [m/s2]
M=0.146;              % Flight Mach Number | V=22.1 [m/s]
SoS=343.2 [m/s]
% e=0.7;

% Power Plant Electrical System

PMax=2700*0.98;
WB=4.41;           % Battery Weight [kg]
Eesp=145;            % Specific Energy [Wh/kg]
MFBatt=WB/W;         % Battery Mass Fraction
nt=0.85;

% Air Properties - ISA

RGases=287.05;       % Gases Constant
ro=1.225;            % Density at sea level [kg/m3]
r=1.4;               % Adiabatic Index of Air

for i=1:3000

    Al(i,:)=i;

if H < 11000

    t_amb = 288.15-0.0065*H;
```

```
% Surroundings Temperature [k]
    p_amb = 101325*(1-0.0000226*H)^(5.256);
% Static Pressure [Pa]
    ro_ambi(i,:) = 1.226*(1-0.0000226*i)^(5.256);
% Density [kg/m^3]
    a_amb = (r*RGases*t_amb)^0.5;
% Speed of Sound [m/s]

else

    t_amb = 271.15-56.5;
% Surroundings Temperature [k]
    p_amb = 22557.74*exp(-(H-11000)/6341.33);
% Static Pressure [Pa]
    ro_amb = 0.363*exp(-(H-11000)/6341.33);
% Density [kg/m^3]
    a_amb = (r*RGases*t_amb)^0.5;
% Speed of Sound [m/s]

end

   V0= M*a_amb;
% Aircraft Speed [m/s]
   Tamb = t_amb * (1+M^2*(r-1)/2);
% Surroundings Temperature
   Pamb = p_amb * (1+M^2*(r-1)/2)^(r/(r-1));
% Surroundings Pressure

end

ro_amb = 1.226*(1-0.0000226*Hth)^(5.256); % Density [kg/m^3]
V0= M*a_amb;          % Aircraft Speed [m/s]

aa=1;

% Aerodynamic Characterization

e=0.83;                      % Oswald's Efficiency Factor

% Kinematic Analysis

Cl=0.185;
n=1.2;
% Ultimate Load Factor
Vs=((2*n*W)/(ro_amb*Sw*Cl))^(1/2)
% Stalling Speed
Dm=(W/(Cl))
% Minimum Drag
MPR=(4*W/3)*((((2*W)/(Sw*ro_amb))*(((3*CD0)/(pi*A*e)^3)^(1/2))
)^(1/2))
```

```
% Minimum Power Required | Ruijgrock 9.28

%% THE TAKEOFF MANEUVER - GROUND RUN

e=0.83;
% Oswald's Efficiency Factor
CD0=0.0310;
% Zero Lift-Drag Coefficient

VMS=Vs
% VS = Minimum Stalling Speed = Vs | Calibrated
VMC=Vs;
% VM = Minimum Control Velocity = Vs
VROT=1.05*VMC;
% VROT = Rotation Speed
VLOF=VROT
% VLOF = Liftoff Velocity | Maximum Speed
VMU=VLOF/1.1;
% VMU = Minimum LiftOff / Unstick Velocity
VCL=1.2*Vs
% VCL = Climbout Velocity | Fig. 16-11
ur=0.02;
% Rolling Friction | 0.02 Concrete | 0.05 Grass
Clg=1.5;
% Clg = Cl @ Ground Cl(6) AoA=6
Cdg=CD0+((Clg^2)/pi*A*e);
% Drag Coefficient at LOF
ClLOF=1.5;
% ClLOF = Cl @ LOF / RCMax  Cl(10) AoA=10
Tr=0.8;
% Mean Thrust | Fig. 9.11 @ Mach Number

% Ground Run Distance [m] - [Ruijgrock 16.7]
sg=((W/Sw)/(ro_amb*g*((ur*(W-
Clg*1/2*ro_amb*VROT^2*Sw))/(1/2*ro_amb*VROT^2*Sw))-
ur*Clg))*log(((Tr/W)-ur)/((Tr/W)-ur-((((ur*(W-
Clg*1/2*ro_amb*VROT^2*Sw))/(1/2*ro_amb*VROT^2*Sw))-
ur*Clg)/(ClLOF))))
% Mean Acceleration [m/s2] - [Ruijgrock 16.8]
ma=(VLOF^2)/sg
% Thrust Required in Ground Run @ 0.7*VLOF - [Ruijgrock 16.3]
Ttmgr=(ma/g)+((((ur*(W-
Clg*1/2*ro_amb*VROT^2*Sw))/(1/2*ro_amb*VROT^2*Sw))-
ur*Clg))*((0.5*ro_amb*0.7*VROT)/(W/Sw))

% Consumed Power - Ground Run
Ptmgr=Ttmgr*Vs
```

```
% Endurance [h*60=min]
Etmgr=(Eesp/g)*MFBatt*nt*((PMax-tmgr)/PMax)*((Clg/Cdg)/VMC)*60
% Range [h*m/s*3600s/h/1000=km]
Rtmgr=(Eesp/g)*MFBatt*nt*((PMax-Ptmgr)/PMax)*((Clg/Cdg))*3.6

Ttmgr=Rtmgr/VMC
Entmgr=Ptmgr*Ttmgr

%% THE TAKEOFF MANEUVER - AIRBORNE PHASE

% Power Available at Takeoff Maneuver Initial Airborne Phase
PAtmap=PMax-Ptmgr;

n=1.4;
% Ultimate Load Factor [R pg.310 | L/W ]
CdLOF=CD0+((ClLOF^2)/pi*A*e);
% Drag Coefficient at LOF
DLOF=CdLOF*1/2*ro_amb*VROT^2*Sw;
% Drag @ LOF | VOp

% Thrust at LOF
Ttmap=(ma/g)+((((ur*(W-
ClLOF*1/2*ro_amb*VLOF^2*Sw))/(1/2*ro_amb*VLOF^2*Sw))-
ur*Clg))*((0.5*ro_amb*VLOF)/(W/Sw))
% Airborne Path Radius [m] [Ruijgrock 16.19]
R=VLOF^2/g*(n-1)
%Screen Height
hs=15
% Flight Path Angle at the Screen
tmfpa=(2*hs/R)^(1/2)
% Airborne Distance
sa=R*tmfpa
% Consumed Power at Airbrone Phase
Ptmap=Ttmap*VLOF

% Endurance [h*60=min]
Etmap=(Eesp/g)*MFBatt*nt*((PAtmap-
Ptmap)/PMax)*((ClLOF/CdLOF)/VLOF)*60

% Range [h*m/s*3600s/h/1000=km]
Rtmap=(Eesp/g)*MFBatt*nt*((PAtmap-
Ptmap)/PMax)*((ClLOF/CdLOF))*3.6

Ttmap=Rtmap/VLOF
Entmap=Ptmap*Ttmap

%% THE TAKEOFF MANEUVER - CLIMB

% Power Available at Takeoff Maneuver Initial Climb
PAtmco=PMax-Ptmgr-Ptmap;
```

```
VCL=1.2*Vs;                % Airspeed Constraint

Clcp=1.5
Cdcp=0.0310+((Clcp^2)/pi*A*e)

ROC=VCL/(g*((n^2)-1)^(1/2))
tmin=(Hth/ROC)*(log(1/(1-(H/Hth))));
% Min. Time

% ROC at Steady Flight [m/s] | Excess Power [W]
ROCsf=(PAtmco)/W
% Minimum Climbing Time [s]
tmin
% Maximum Climb Angle
maxcaap=abs((Tr/W)-(1/(Clcp/Cdcp)))
% Consumed Power at Climb
Ptmcp=VCL*sin(maxcaap*0.0174533)*W

% Endurance [h*60=min]
Etmcp=(Eesp/g)*MFBatt*nt*((PAtmco-
Ptmcp)/PMax)*((Clcp/Cdcp)/VCL)*60
% Range [h*m/s*3600s/h/1000=km]
Rtmcp=(Eesp/g)*MFBatt*nt*((PAtmco-
Ptmcp)/PMax)*((Clcp/Cdcp))*3.6

Ttmcp=Rtmcp/VCL
Entmcp=Ptmcp*Ttmcp

%% CRUISE CONDITION

% Power Available at Initial Cruise Condition
PAtmco=PMax-Ptmgr-Ptmap-Ptmcp;

L=W;
% Steady Level Flight - Cruise Consideration
q=1/2*ro_amb*(V0^2);
% Dynamic Pressure [m/s2]
Cl=L/(q*Sw);
% Lift Coefficient [.]
e=0.83;
% Oswald's Efficiency Factor
CD0=0.0110;
% Zero Lift-Drag Coefficient
Cd=CD0+((Cl^2)/pi*A*e);

%%% Aircraft Velocities
V=(((2*W)/(Sw*ro_amb*Cl))^(0.5));
D=1.1*(CD0*(1/2)*ro_amb*(V^2)*Sw)+((W^2)/((1/2)*ro*(V^2)*Sw));
```

```
%%% POWER REQUIRED | Avanzini

Pav=10;             % Avionics [W] Aprox. Value | Ref.
Pp=10;              % Payload [W] Aprox. Value  | Ref.
Pcr=Pav+Pp+(CD0*(1/2)*ro_amb*V^3*Sw)+((W^2)/(pi*A*e*(1/2)*ro_a
mb*V*Sw));

% Endurance [h*60=min]
Ecr=(Eesp/g)*MFBatt*nt*((fU-Pcr)/PMax)*((Cl/Cd)/V)*60
% Range [h*m/s*3600s/h/1000=km]
Rcr=(Eesp/g)*MFBatt*nt*((fU-Pcr)/PMax)*((Cl/Cd))*3.6

Tcr=Rcr/V
Encr=Pcr*Tcr

%% THE AIRBORNE DISTANCE - LADING MANEUVER

% Power Available at Landing Maneuver Initial Airborne Phase
PAtmco=PMax-Ptmgr-Ptmap-Ptmcp-Pcr;

e=0.75;                 % Oswald's Efficiency Factor
CD0=0.1010;             % Zero Lift-Drag Coefficient

% Steady Approach
VA=Vs;
% Steady Approach Velocity over hslm
nA=1.2;
% Ultimate Load Factor at Steady Approach
Cla=2;
% Lift Coefficient at Steady Approach @ 1.3*Vs
Cda=CD0+((Cla^2)/pi*A*e);
rda=1/(sin((Cda/Cla)*0.0174533))
% Flight Path Angle [Ruijgrock 16.44]
hslm=15;
% Screen in Landing Maneuver
Rlm=VA^2/(g*(1.2-1))
% Radius of Curvature [Ruijgrock 16.46]
stlm=Rlm*rda
% Horizontal Distance [m]

% Touchdown
VT=1.15*Vs          % Radius of Curvature | Ruijgrock 16.54
Cdt=Cda;            % Drag Coefficient at Touchdown @ 1.15*Vs
Clt=Cla;            % Lift Coefficient at Touchdown @ 1.15*Vs

% Endurance [h*60=min]
Elmap=(Eesp/g)*MFBatt*nt*((PAtmco)/PMax)*((Cla/Cda)/VA)*60
% Range [h*m/s*3600s/h/1000=km]
Rlmap=(Eesp/g)*MFBatt*nt*((PAtmco)/PMax)*((Cla/Cda))*3.6
```

```
Tlmap=Rlmap/VA

%% THE LANDING GROUND RUN | Section 16.7

% Power Available at Landing Maneuver Initial Ground Run
PAtmco=PMax-Ptmgr-Ptmap-Ptmcp-Pcr;

ub=0.02 ;
% Friction Coefficient due to Slip Ratio [R Fig 16.17]
Clg=Cla;
% Clg = Cl @ Ground Cl(6) AoA=6
Cdg=Cda;
% Ground Drag Coefficient | Cdg = Cd @ Cd(6) AoA=6
Dgmax=Cda*1/2*ro_amb*VT^2*Sw;
% Maximum Ground Drag Coefficient
VB=Vs;
Z=(Cdg-ub*Clg)/(ub*Clt);

algr=(g/W)*(-Cdg*1/2*ro_amb*V)
% Landing Ground Run Acceleration [Ruijgrock 16.67]
VBgr=(W-(Dgmax/ub))/(Clg*1/2*ro_amb*Sw)
% Distance for Brake Velocity [Ruijgrock 16.62]
sb1=((VT^2)/(2*g*ub*Z))*log((1+Z)/(1+Z*(VB^2/VT^2)))
% Skidding [Ruijgrock 16.66]
sb2=((W)/(Cdg*ro_amb*g*Sw))*log(((Cdg*(1/2)*ro_amb*(VB^2)*Sw)/
(Dgmax))+1)
% Brake Distance [Ruijgrock 16.69]
sgl=sb1+sb2+stlm

% Endurance [h*60=min]
Elmgr=(Eesp/g)*MFBatt*nt*((PAtmco)/PMax)*((Clg/Cdg)/VB)*60
% Range [h*m/s*3600s/h/1000=km]
Rlmgr=(Eesp/g)*MFBatt*nt*((PAtmco)/PMax)*((Clg/Cdg))*3.6

Tlmgr=Rlmgr/VB

%% POWER EVALUATION

%POWER REQUIRED
PRTM=Ptmgr+Ptmap+Ptmcp;
% Power Required Takeoff Maneuver
PRCC=Pcr;
% Power Required Cruise Condition
PRT=PRTM+PRCC

% POWER AVAILABLE
PAT=PMax

% POWER REMAINING
PFR=PAT-PRT
```

```
% Endurance
E=Etmgr+Etmap+Etmcp+Ecr+Elmap+Elmgr

% Range
R=Rtmgr+Rtmap+Rtmcp+Rcr+Rlmap+Rlmgr

% Energy
En=Entmgr+Entmap+Entmcp+Encr %+Enlmap+Enlmgr

figure
title('GENERAL POWER ASSESSMENT')
G=[PRTM PRCC PFR];
pie(G)
legend('Takeoff Maneuver','Cruise','Non-Consumed Power')
```